Lesson 13:

Nanoporous Systems

(Nanoporous Systems: introduction and general concepts; Importance of nanoporous metals; Nanoporous gold: properties and applications; Fabrication of nanoporous gold by the dealloying processes of bimetallic alloys: basic principles, thermodynamics and kinetics parameters; composition control, porosity control; Porous gold nannostructures)

Nanoporous Au

State of Art: Nanoporous Au Leafs and Films

Nanoporous Gold Leaf: "Ancient Technology"/Advanced Material**

By *Yi Ding*, *Young-Ju Kim*, and *Jonah Erlebacher**

Adv. Mater. 2004, 16, No. 21, November 4

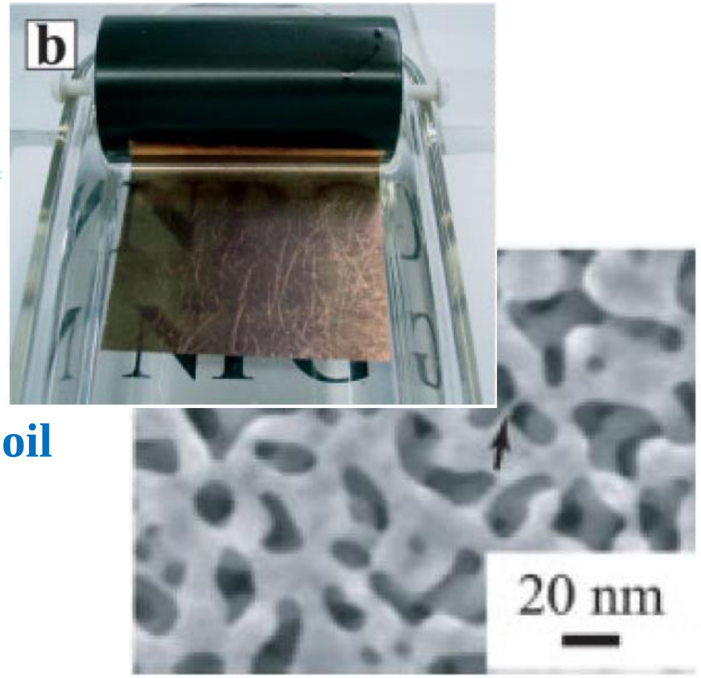

Free-standing Nanoporous Au Foil

ARTICLE

Received 23 Jan 2013 | Accepted 5 Aug 2013 | Published 29 Oct 2013 DOI: 10.1038/ncomms3400 OPEN

Green chemistry and nanofabrication in a levitated Leidenfrost drop

Ramzy Abdelaziz[1], Duygu Disci-Zayed[1], Mehdi Keshavarz Hedayati[1], Jan-Hendrik Pöhls[1], Ahnaf Usman Zillohu[2], Burak Erkartal[3], Venkata Sai Kiran Chakravadhanula[3,†], Viola Duppel[4], Lorenz Kienle[3] & Mady Elbahri[1,2]

NATURE COMMUNICATIONS | 4:2400

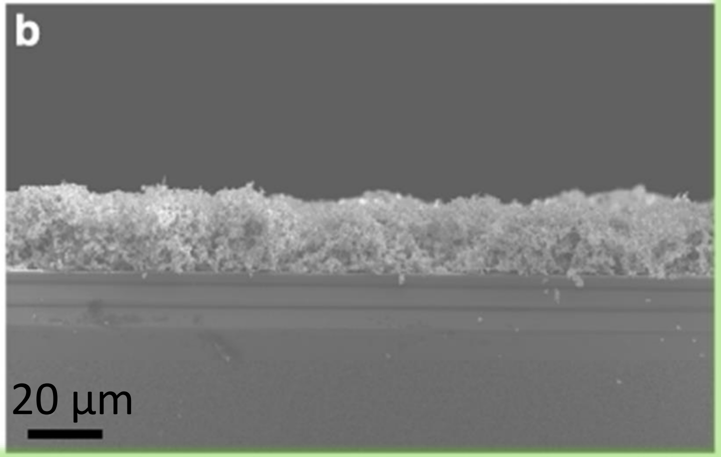

Substrate-supported Nanoporous Au Film

Characteristics

- ✓ Three-Dimensional Structure
- ✓ Localized Surface Plasmon
- ✓ High Surface Area (~10 m^2/g)
- ✓ Electrochemical Properties
- ✓ Size-Dependent Properties

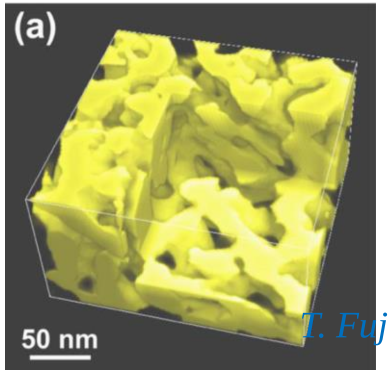

T. Fujita et al., Appl. Phys. Lett. 92, 251902 (2008)

Nanoporous Au

State of Art: Nanoporous Au Leafs and Films-Applications

APPLIED PHYSICS LETTERS **98**, 093701 (2011)

Localized surface plasmon resonance of nanoporous gold

Xingyou Lang,[1] Lihua Qian,[1] Pengfei Guan,[1] Jian Zi,[2] and Mingwei Chen[1,a)]
[1]*WPI Advanced Institute for Materials Research, Tohoku University, Sendai 980-8577, Japan*
[2]*Department of Physics, Surface Physics Laboratory, Fudan University, Shanghai 200433, China*

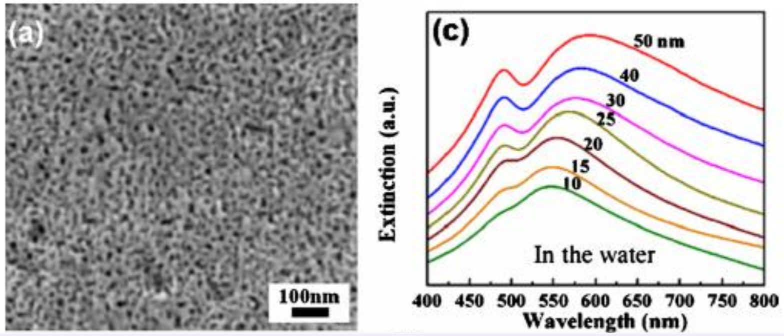

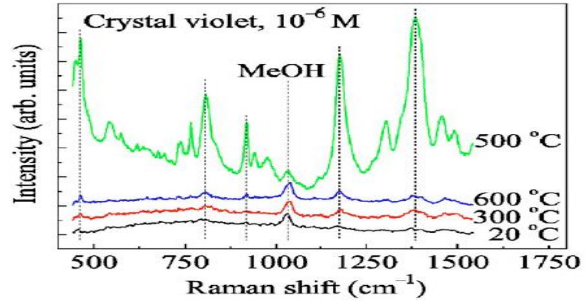

APPLIED PHYSICS LETTERS **89**, 053102 (2006)

Surface-enhanced Raman scattering on nanoporous Au

S. O. Kucheyev,[a)] J. R. Hayes, J. Biener, T. Huser,[b)] C. E. Talley, and A. V. Hamza
Lawrence Livermore National Laboratory, Livermore, California 94551

ELSEVIER
Available online at www.sciencedirect.com
ScienceDirect
Scripta Materialia 65 (2011) 17–20
Scripta MATERIALIA
www.elsevier.com/locate/scriptamat

Nanoporous gold for enzyme-free electrochemical glucose sensors

L.Y. Chen, X.Y. Lang, T. Fujita and M.W. Chen*
WPI Advanced Institute for Materials Research, Tohoku University, Sendai 980-8577, Japan

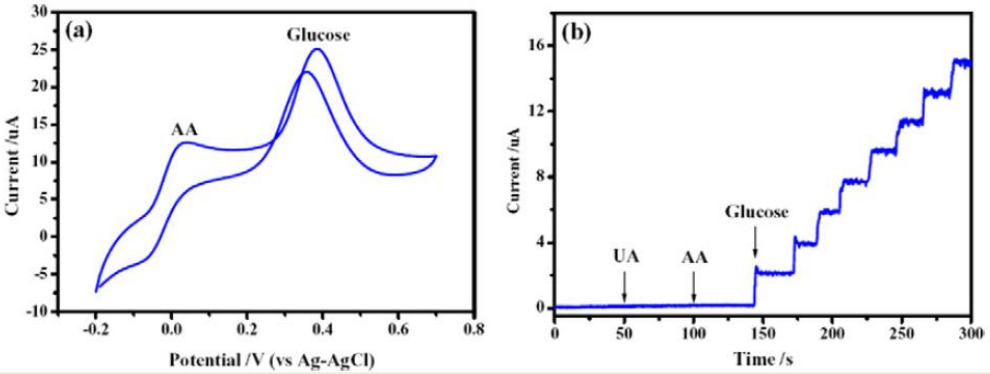

1) Nanoporous Au

Fabrication by Dealloying a Au-X Bimetallic Alloy

Nanoporous Au can be easily prepared from Au-X alloys of suitable composition by using a simple dealloying process of the X less noble elements

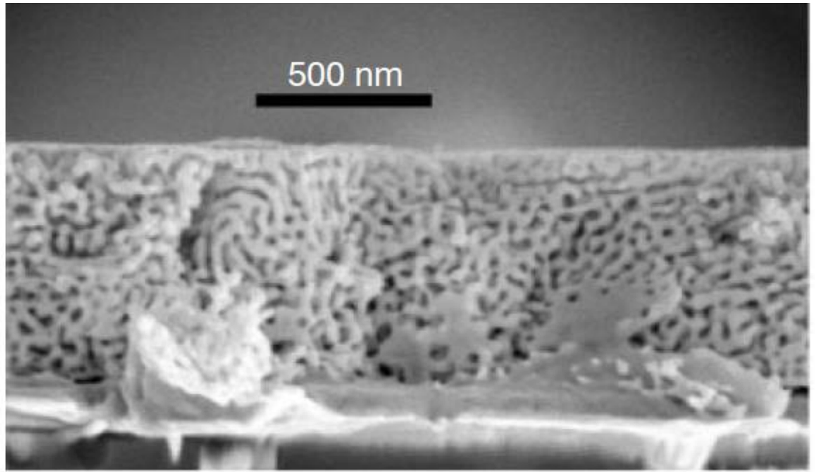

Requirements

- ✓ **Au-X: HOMOGENEOUS binary solid solution**
- ✓ **High difference in Au/X-ion electrode potential**

AuAg, AuCu

J. Erlebacher et al, Nature 410, 450 (2001)

1) Nanoporous Au

Perspectives: Porous Au Nanostructures

Porous Au nanostructures possess a much higher surface-to-volume ratio than bulk nanoporous Au leafs and films .

They are expected to broaden the range of applications for nanoporous Au due to their two-level nanostructures

(pores size ~10 nm and structures size ~100 nm)

Nanoporous Au Particles

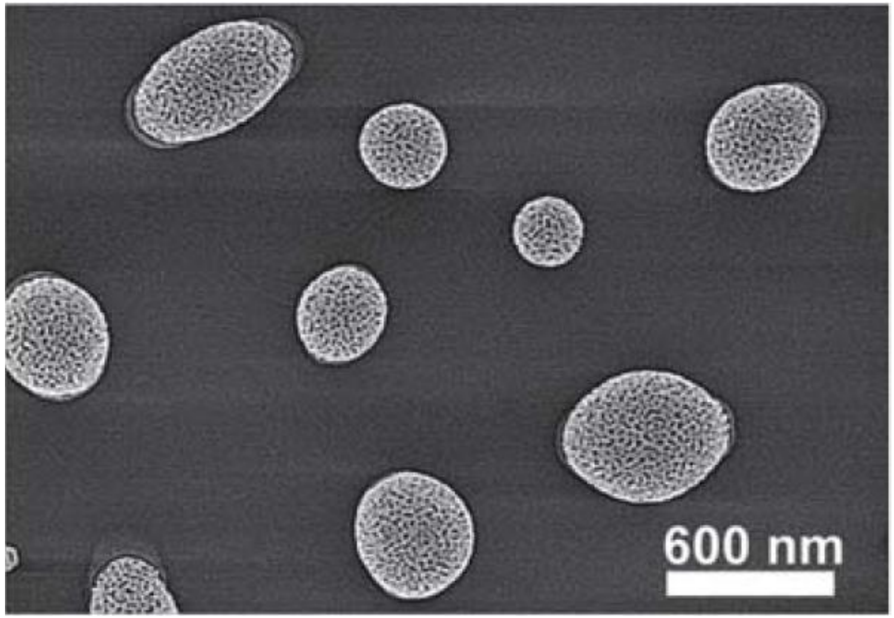

D. Wang et al., J. Mater. Chem. 22, 5344 (2012)

Nanoporous Au Wires

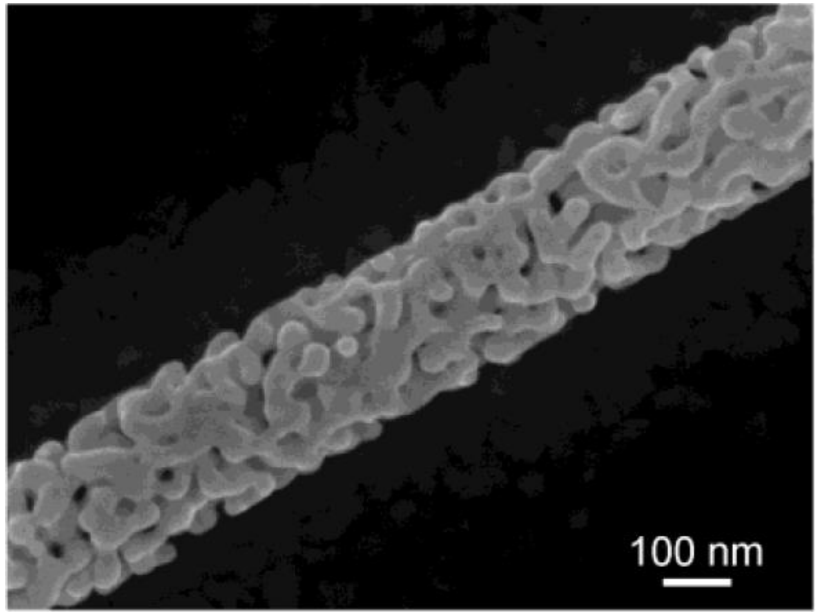

C. Ji et al., J. Phys. Chem. B 107, 4494 (2003)

A **homogeneous mixture** is a solid, liquid, or gaseous mixture that has the same proportions of its components throughout any given sample. Conversely, a **heterogeneous mixture** has components whose proportions vary throughout the sample

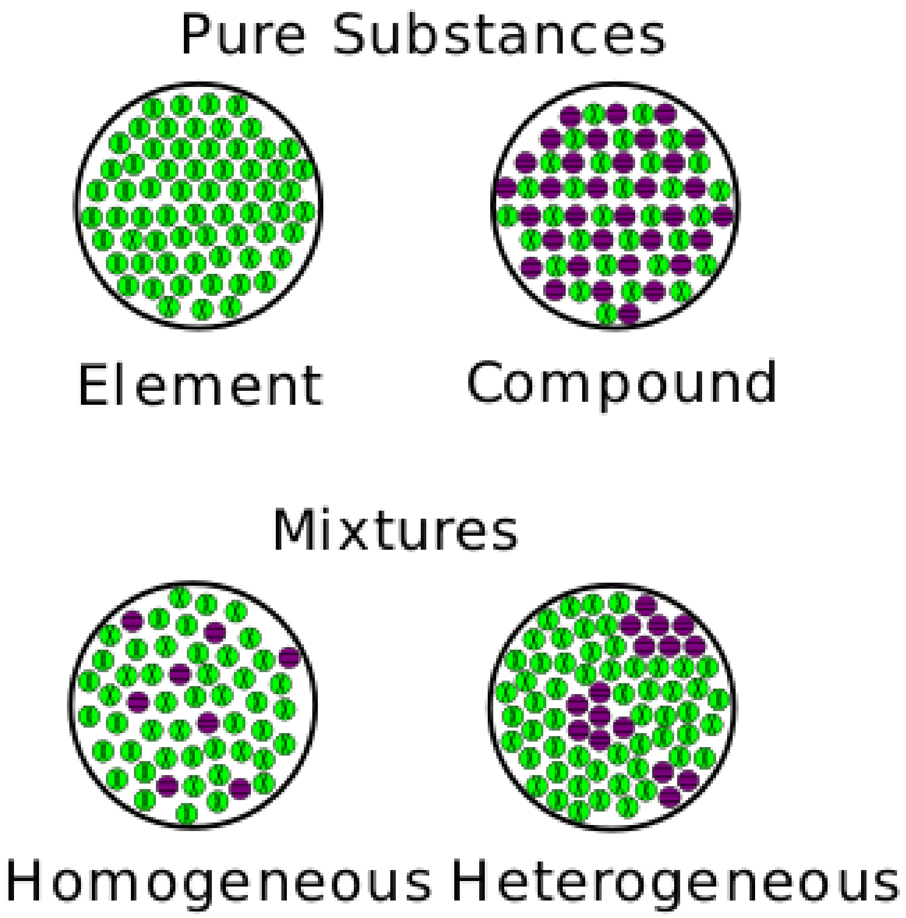

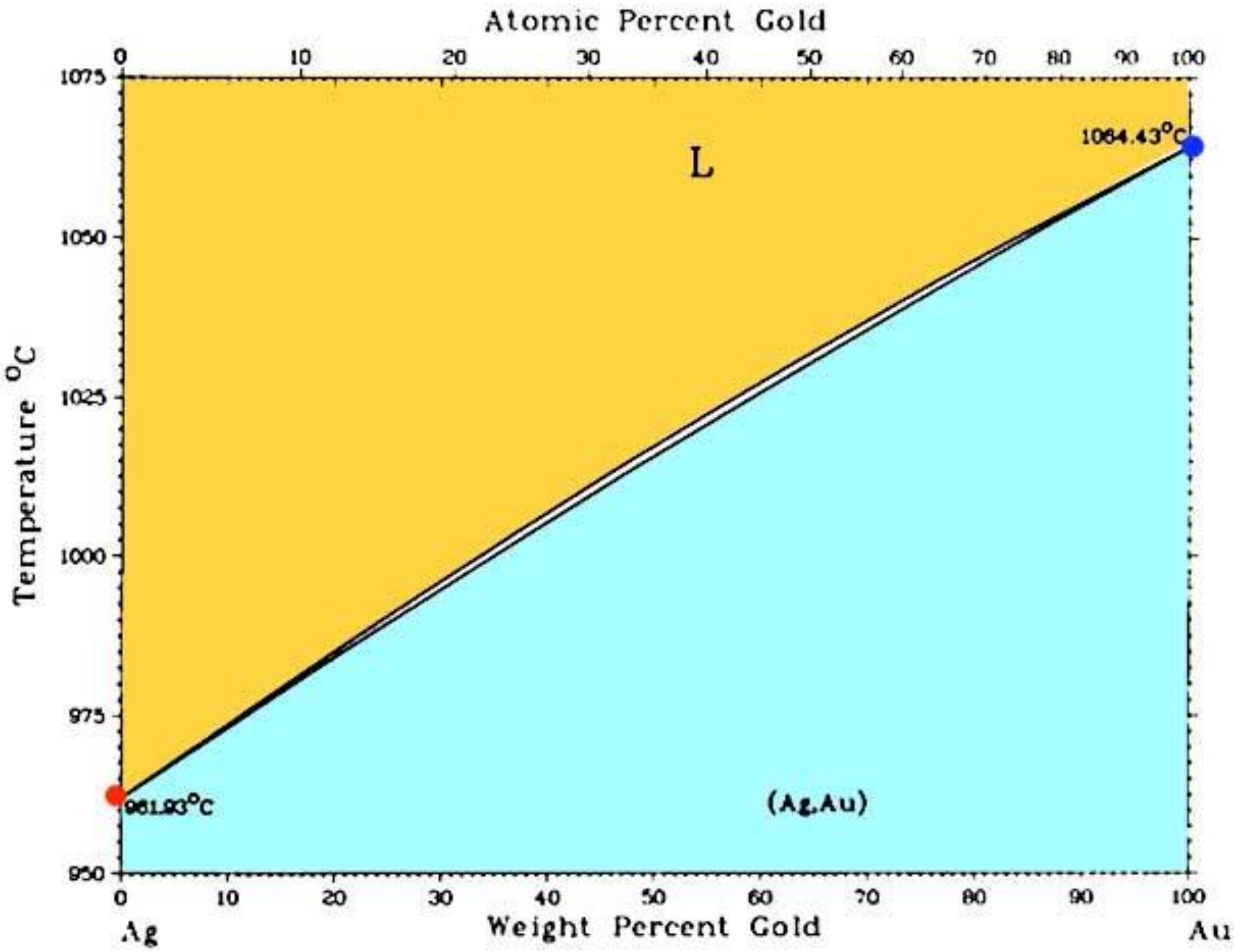

Phase diagram for Au-Ag is a simple lens type. the FCC phase shows complete solid solubility

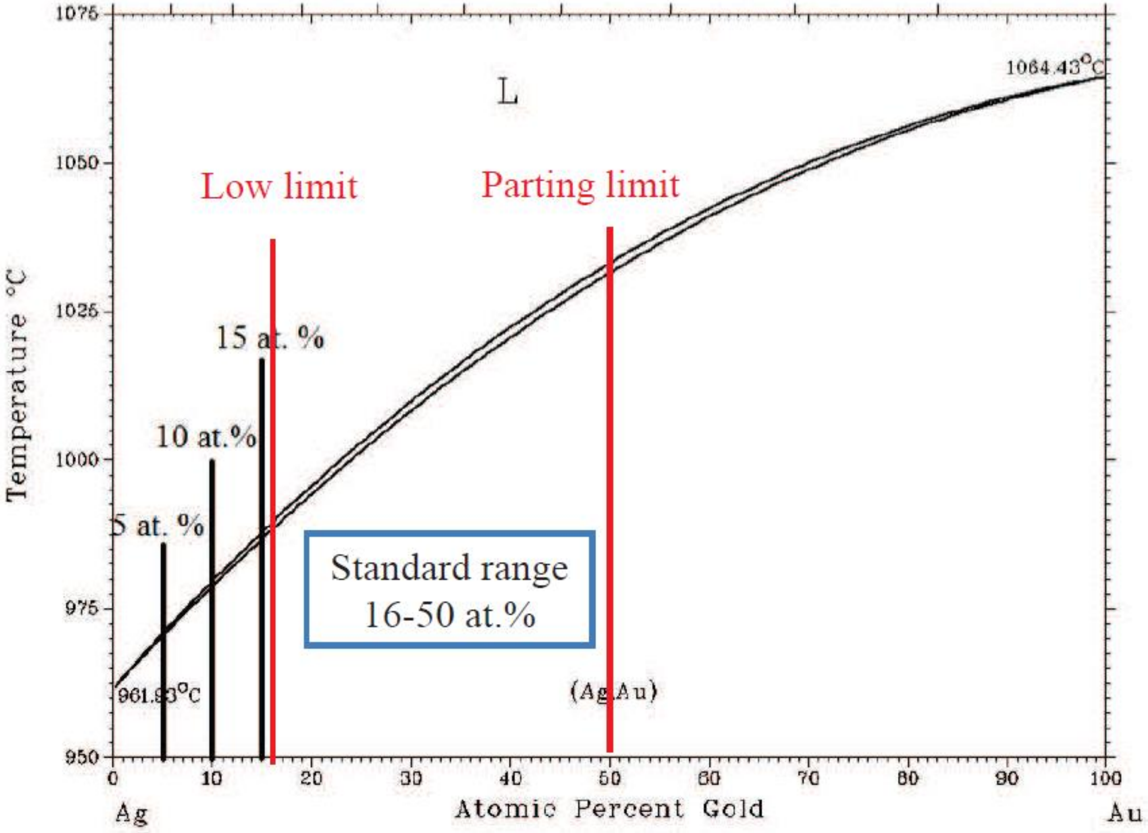

Figure 2.7: Phase diagram of the binary Ag-Au alloy. Three regions are classified based on the initial alloy composition to prepare nanoporous gold. [51, 52]. Reprinted with permission of ASM International. All rights reserved. www.asminternational.org.

Figure 2.7 shows the phase diagram of binary Ag-Au alloy, and it is divided into three different regions based on the alloy composition to prepare NPG by dealloying: dilute composition region, standard composition region, and parting limit region [48, 52].

For all the alloys that can be dealloyed, a parting limit can be observed. The parting limit is a boundary where dealloying stops at a certain depth due to the MNEs passivation when the composition of MNEs exceeds a certain value during dealloying. Typically, it is close to 50 at.% Au for Ag-Au alloy which is shown in Figure 2.7 as parting limit. The origin of parting limit is that the enrichment of MNEs will block the pathway which connects the electrolytes and LNEs. Therefore, the whole dealloying process is hindered by the passivation of MNE enriched surface and no more dissolution of LNEs. The parting limit determines the upper limit of content of MNEs that can be selected to prepare NPG by dealloying. When the Au content is higher than the parting limit, it is in the parting limit region.

The standard composition region refers to that a monolithic body of nanoporous structure can be prepared from this composition region with an empirical composition range of 16 - 50 at.% Au [52]. It is the composition region between parting limit and low limit. For Ag-Au solid solution system, crack-free NPG can be fabricated from this composition range which is an ideal candidate for mechanical test [40, 41, 53].

When the Au composition is lower than 16 at.%, the samples tend to fall into small pieces during dealloying, therefore, losing its integrity [52]. Here, this composition range is defined as the dilute composition region which is below the low limit showing in Figure 2.7. Normally, this composition range is not desirable in making NPG. Interestingly, Ateya *et al.* studied the

Dealloying

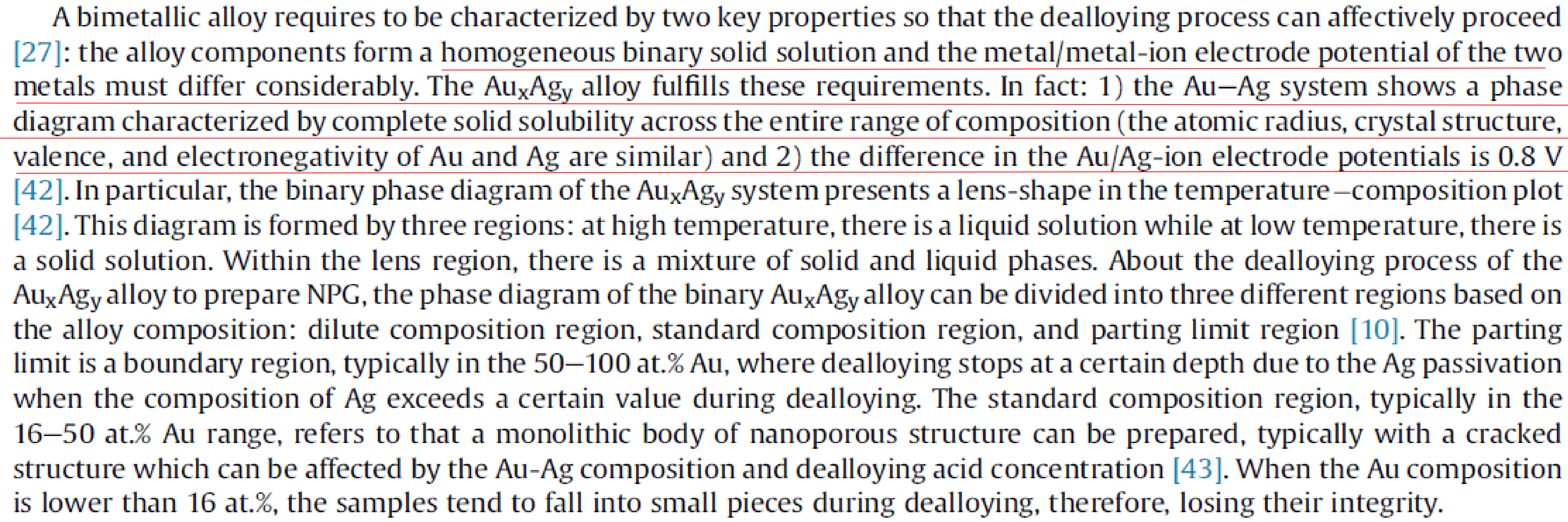

A bimetallic alloy requires to be characterized by two key properties so that the dealloying process can affectively proceed [27]: the alloy components form a homogeneous binary solid solution and the metal/metal-ion electrode potential of the two metals must differ considerably. The Au_xAg_y alloy fulfills these requirements. In fact: 1) the Au–Ag system shows a phase diagram characterized by complete solid solubility across the entire range of composition (the atomic radius, crystal structure, valence, and electronegativity of Au and Ag are similar) and 2) the difference in the Au/Ag-ion electrode potentials is 0.8 V [42]. In particular, the binary phase diagram of the Au_xAg_y system presents a lens-shape in the temperature–composition plot [42]. This diagram is formed by three regions: at high temperature, there is a liquid solution while at low temperature, there is a solid solution. Within the lens region, there is a mixture of solid and liquid phases. About the dealloying process of the Au_xAg_y alloy to prepare NPG, the phase diagram of the binary Au_xAg_y alloy can be divided into three different regions based on the alloy composition: dilute composition region, standard composition region, and parting limit region [10]. The parting limit is a boundary region, typically in the 50–100 at.% Au, where dealloying stops at a certain depth due to the Ag passivation when the composition of Ag exceeds a certain value during dealloying. The standard composition region, typically in the 16–50 at.% Au range, refers to that a monolithic body of nanoporous structure can be prepared, typically with a cracked structure which can be affected by the Au-Ag composition and dealloying acid concentration [43]. When the Au composition is lower than 16 at.%, the samples tend to fall into small pieces during dealloying, therefore, losing their integrity.

The Au-Ag system has been the most commonly used alloy for synthesizing np-Au, due to (i) availability of etching techniques with high selectivity for silver; (ii) complete solid solubility across all compositions; and (iii) mechanical compatibility (e.g., similar yield stress, thermal expansion, etc.)

3.3. Dissolution Methods

Nitric acid is commonly used to dealloy Au-Ag in order to produce np-Au and has the advantage of circumventing the use of electrochemical dissolution circuitry. However, this comes with the trade-off of diminished control of pore size. Alternatively, application of an anodic potential during dealloying in perchloric acid increases the silver dissolution rate compared to the gold diffusion rate, and hence results in finer porosity. The latter method has a greater number of controllable parameters, such as electrolyte temperature, critical potential (potential where the less noble constitute begins to dissolve), electrolyte composition, *etc.* Several groups have investigated key parameters during this

Dealloying and Dealloyed Materials

Ian McCue, Ellen Benn, Bernard Gaskey, and Jonah Erlebacher*

Department of Materials Science and Engineering, Johns Hopkins University, Baltimore, Maryland 21218; email: Jonah.Erlebacher@jhu.edu

Nanoporous Au can be easily prepared from Au-X alloys of suitable composition by using a simple dealloying process of the X less noble elements

Au_xAg_y Alloy Film

Dealloying in HNO_3

Nanoporous Au

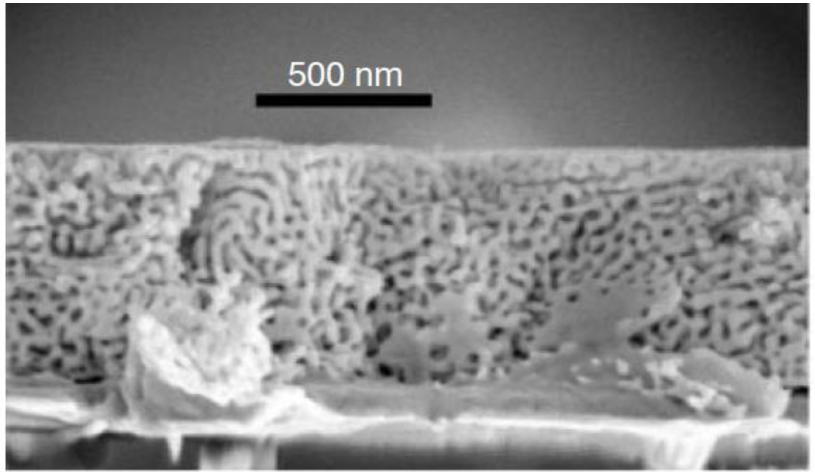

Requirements

- ✓ Au-X: HOMOGENEOUS binary solid solution
- ✓ High difference in Au/X-ion electrode potential

AuAg, AuCu

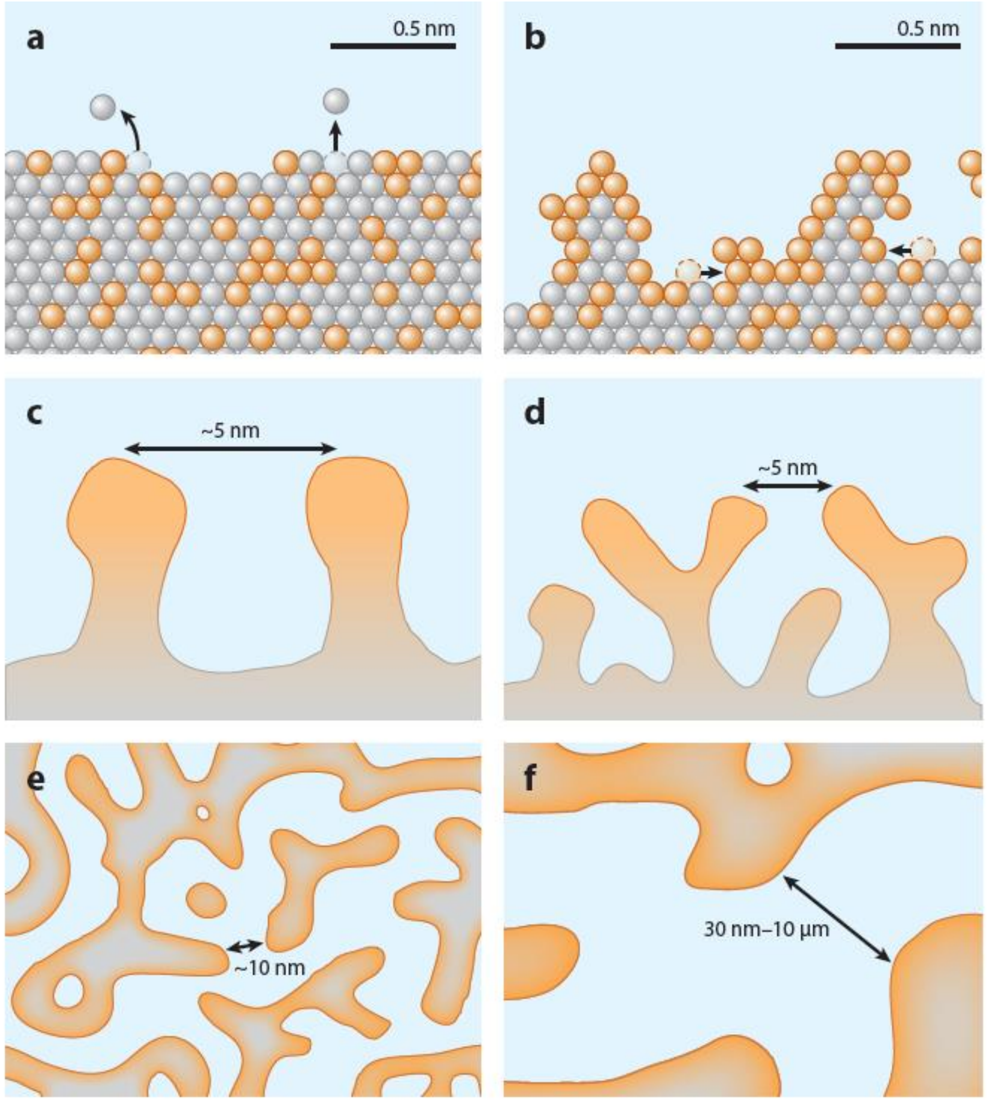

Figure 2

Working model for porosity evolution in dealloying in the Ag-Au alloy system (Ag, *gray*; Au, *orange*). (*a*) The rate-limiting step is the formation of terrace vacancies, which then grow into lateral vacancy clusters. (*b*) As dissolution proceeds layer by layer, surface diffusion passivates low-coordination sites with Au, leading to surface roughening. (*c*,*d*) As dealloying continues, there is insufficient Au to totally passivate the increasing surface area, leading to undercutting and bifurcation of ligaments. (*e*) The result of this process is a bicontinuous porous structure in which ligaments have Au-rich surfaces and Ag-rich interiors. (*f*) As coarsening increases the length scale of the initial structure, residual Ag atoms are exposed and dissolved, leaving a final structure with much reduced Ag content.

3.1. Porosity Formation

Despite the first observation of porosity evolution in np-Au during early 1990s (an early report of pattern formation during dealloying dates back to 1920s [23]), the actual mechanisms that played a pivotal role were not well-studied until more than a decade later. Erlebacher *et al.* used an elegant kinetic model to describe the nanoporosity formation in a Au-Ag alloy, using only diffusions of silver and gold, and a dissolution of silver [24,25]. They suggested that spinodal decomposition arranges the gold atoms in two-dimensional clusters at the surface of the alloy, as silver is dissolved. Through this process, the new underlying alloy is constantly exposed to the electrolyte setting the length scale of the pore morphology. Figure 2 schematically summarizes the proposed mechanism.

Figure 2. Illustration of porosity formation during dealloying: (a) lateral removal of less noble atoms (uncolored) leading to clustering of noble atoms (shaded) on surface; (b) supplied with remaining noble atoms from dissolution, clusters coarsen until the next alloy layer is attacked, as the characteristic length $<\lambda>$ appears; (c) noble atom-capped hills form as the second layer of alloy dissolves, while the characteristic length between hills remains the same; (d) less noble atoms can accumulate at the bases of hills, since their perimeters are widening, without changing the characteristic length; (e) undercutting of hills (compared the original morphology denoted with a dashed line) and increase in average distance between hills measured along the alloy-electrolyte interface; (f) new noble atom hills nucleate as the hill-hill distance along the alloy-electrolyte distance is approximately twice the characteristic length. [Reproduced with permission from *J. Electrochem. Soc.* **2004**, *151*, C614–C626. © 2004, The Electrochemical Society].

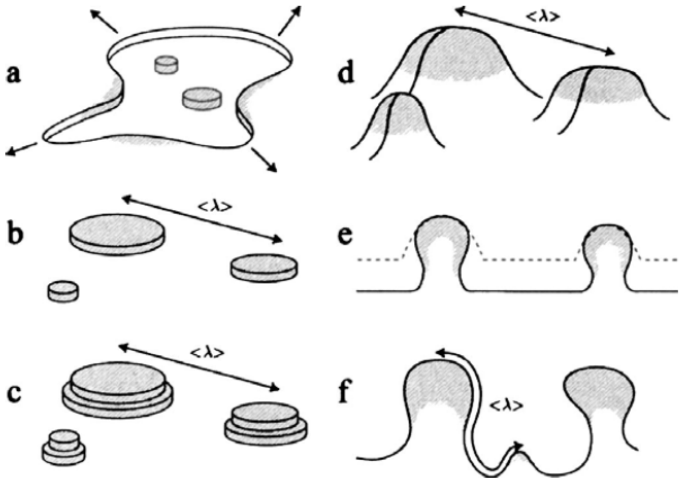

Materials **2009**, *2*, 2188-2215; doi:10.3390/ma2042188

OPEN ACCESS

materials

ISSN 1996-1944

www.mdpi.com/journal/materials

Review

Nanoporous Gold: Fabrication, Characterization, and Applications

Erkin Seker [1],*, Michael L. Reed [2] and Matthew R. Begley [2,3,4]

Formazione di “instabiltà”

Principi di formazione delle nanocavità→ cause dei processi di dissociazione dell’argento

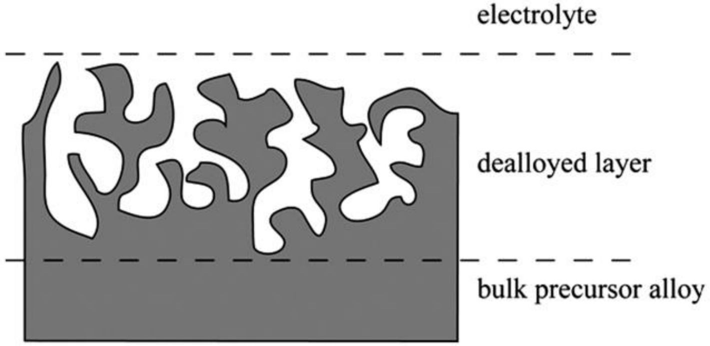

Gli atomi di Ag vengono attacati “contemporanemanete”

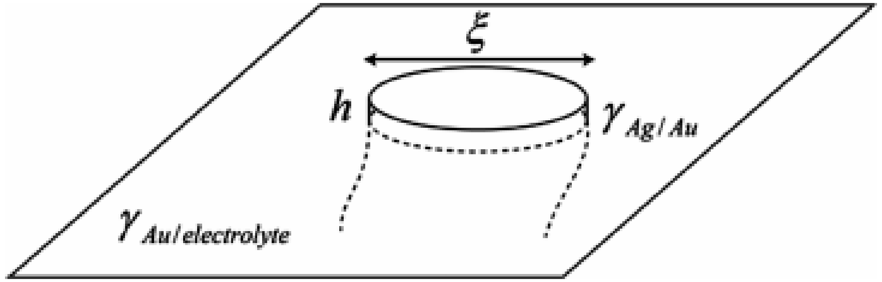

E_c deriva dall’ energia necessaria alla formazione di nuove superfici

Dopo averli staccati tutti si ha un’energia Residua che crea una nuova superficie:

$$\Delta F = NkT \ln\left(a_{\mathrm{Ag^+}}/a_{\mathrm{Ag}}\right) - h\pi\xi\gamma_{\mathrm{Ag/Au}} + h\pi\xi\gamma_{\mathrm{Au/elec}\text{-}}$$

Nano-fabricazioni di NPG

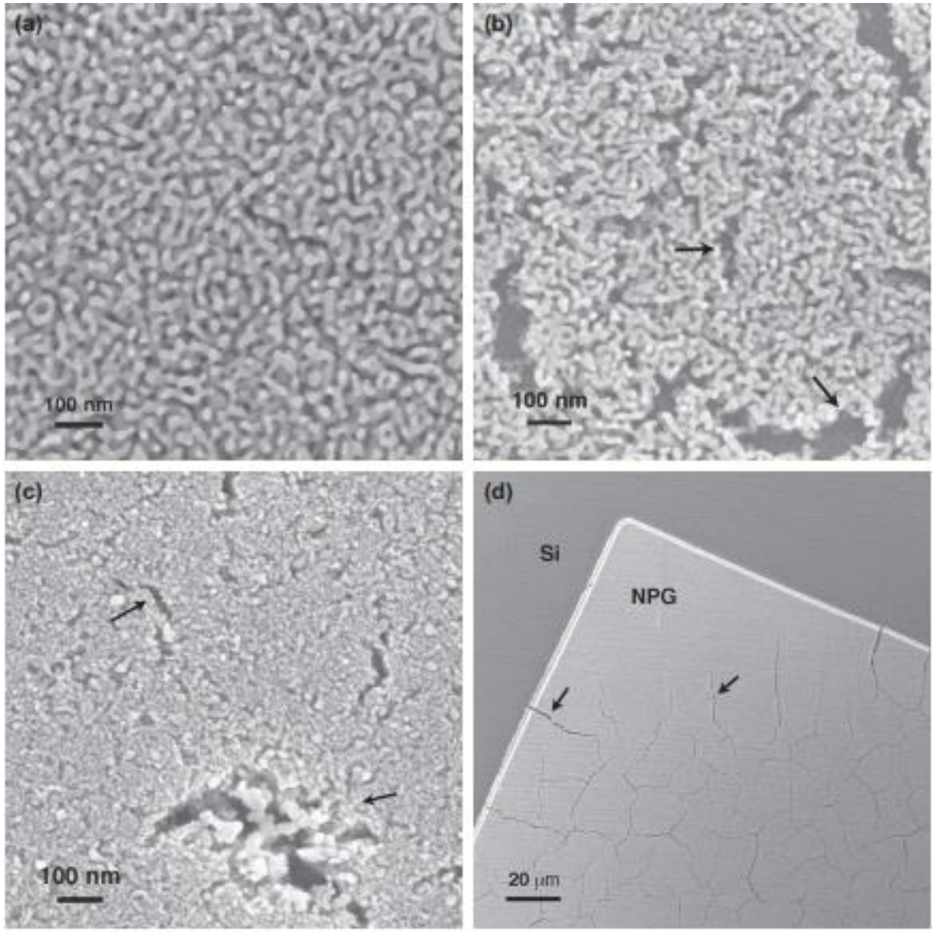

Ovviamente rimangono valide le condizione enunciate prima (limite di partizione, potenziale di attivazione ecc..).

Altra condizione importante per la formazione delle nanoporosità è appunto la temperatura, che come vediamo nella figura, fa si che le nostre strutture abbiano un disordine maggiore (e quindi pori più piccoli, (a)) e man mano che la temperatura aumenta, in concomitanza al dealloying dai metalli secondari (come l’argento), la dimensione dei pori diminuisce sempre di più fino a raggiungere delle semplici frammentazioni superficiali che compromettono anche alcune applicazioni del film.

La lunghezza critica del film di NPG è dettata dalla legge:

$$\boxed{h_{\mathrm{f}}^{\mathrm{cr}} = \frac{2\Gamma_{\mathrm{f}} E_{\mathrm{f}}}{\pi c_{\mathrm{f}}^{2} \sigma_{\mathrm{m}}^{2}},}$$

APPLIED PHYSICS LETTERS **91**, 083105 (2007)

Ultrafine nanoporous gold by low-temperature dealloying and kinetics of nanopore formation

L. H. Qian and M. W. Chen[a)]
Institute for Materials Research, Tohoku University, Sendai 980-8577, Japan

acteristic length of nanoporous gold. Based on the surface diffusion controlled coarsening mechanism, the diffusivity (D_s) of gold atoms at each etching temperature can be estimated by the equation[19]

$$\boxed{D_s = \frac{d(t)^4 kT}{32\gamma t a^4},} \qquad (2)$$

where k is Boltzmann constant, γ is surface energy, t is the etching time, and a is the lattice parameter. According to the parameters compiled in Ref. 14 and measured by this study, the surface diffusivity of gold in electrolyte at −20, 0, and 25 °C are estimated to be 9.0×10^{-22}, 1.5×10^{-20}, and 2.0×10^{-19} m^2/s, respectively. Therefore, slight temperature

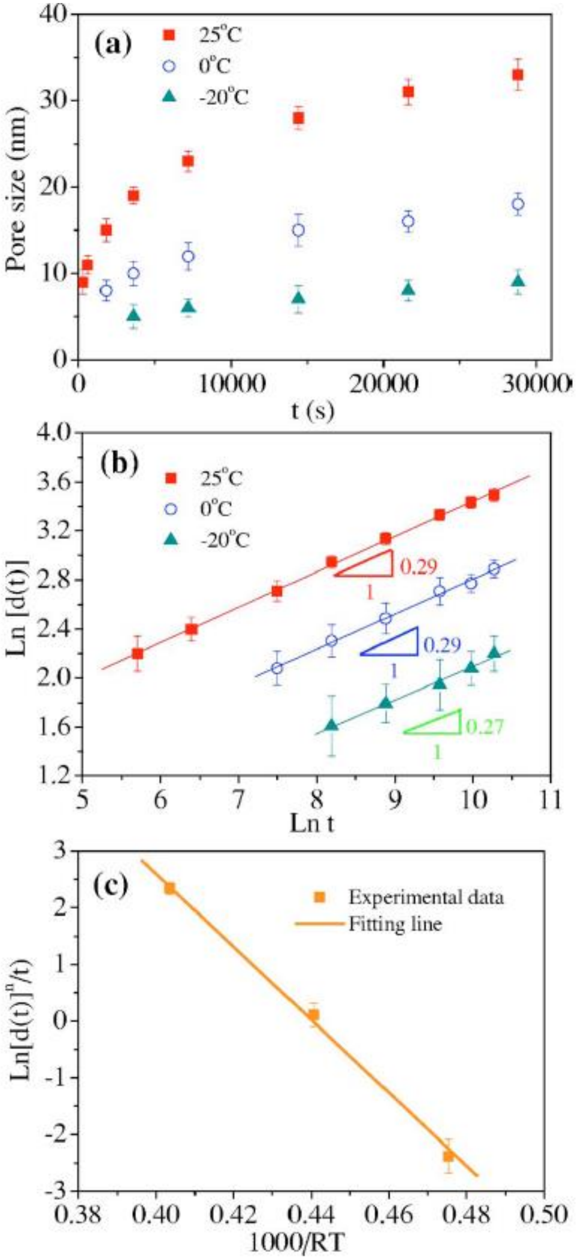

FIG. 1. (Color online) Evolution of nanopore size with etching time and temperature. (a) Correlation between nanopore size and time at various etching temperatures. (b) Measurements of the coarsening exponent by plotting $\ln[d(t)]$ vs $\ln t$ at each etching temperature. (c) Estimation of the activation energy for the nanopore formation.

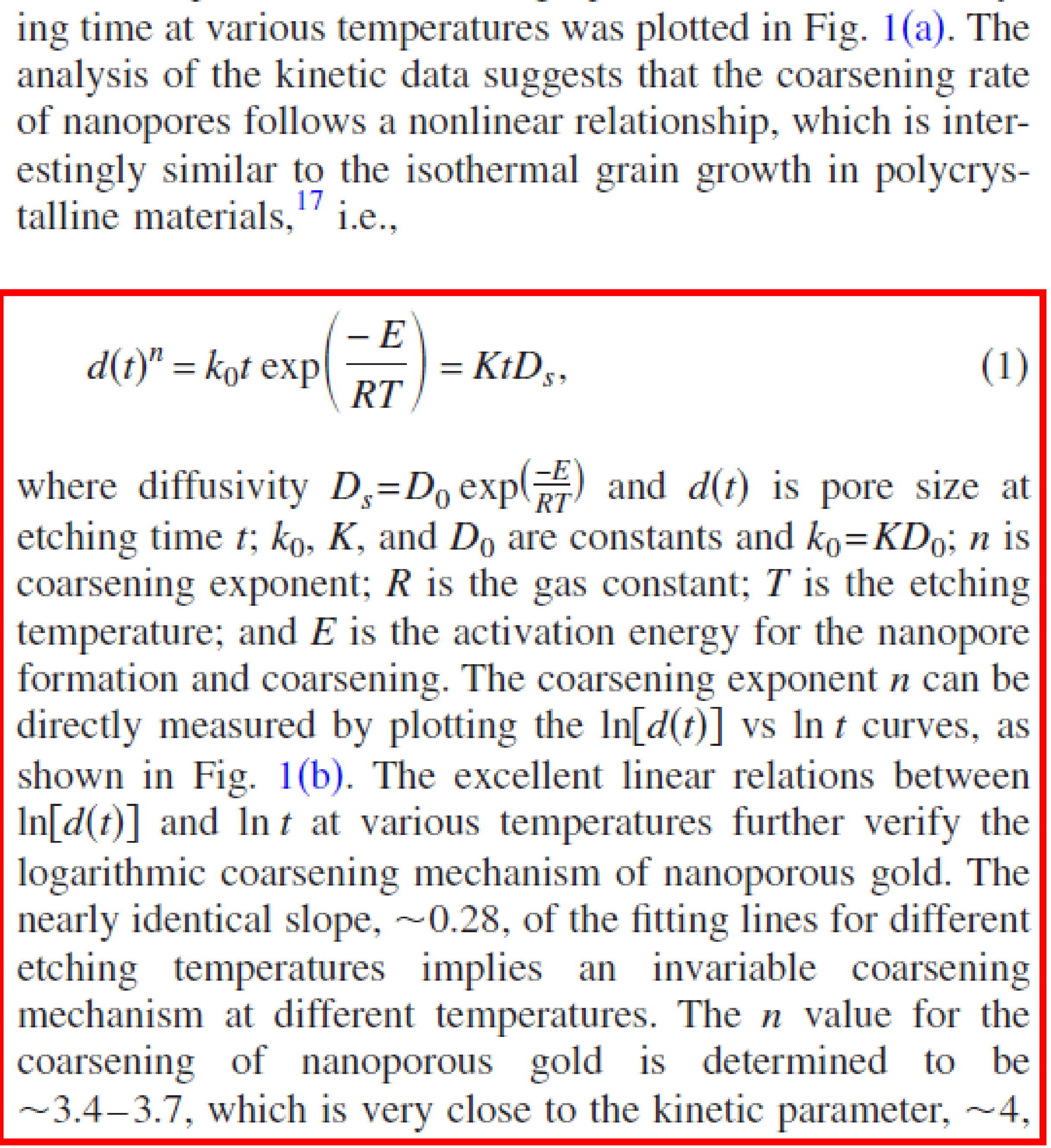

ing time at various temperatures was plotted in Fig. 1(a). The analysis of the kinetic data suggests that the coarsening rate of nanopores follows a nonlinear relationship, which is interestingly similar to the isothermal grain growth in polycrystalline materials,[17] i.e.,

$$d(t)^n = k_0 t \exp\left(\frac{-E}{RT}\right) = KtD_s, \qquad (1)$$

where diffusivity $D_s = D_0 \exp(\frac{-E}{RT})$ and $d(t)$ is pore size at etching time t; k_0, K, and D_0 are constants and $k_0 = KD_0$; n is coarsening exponent; R is the gas constant; T is the etching temperature; and E is the activation energy for the nanopore formation and coarsening. The coarsening exponent n can be directly measured by plotting the $\ln[d(t)]$ vs $\ln t$ curves, as shown in Fig. 1(b). The excellent linear relations between $\ln[d(t)]$ and $\ln t$ at various temperatures further verify the logarithmic coarsening mechanism of nanoporous gold. The nearly identical slope, ~0.28, of the fitting lines for different etching temperatures implies an invariable coarsening mechanism at different temperatures. The n value for the coarsening of nanoporous gold is determined to be ~3.4–3.7, which is very close to the kinetic parameter, ~4,

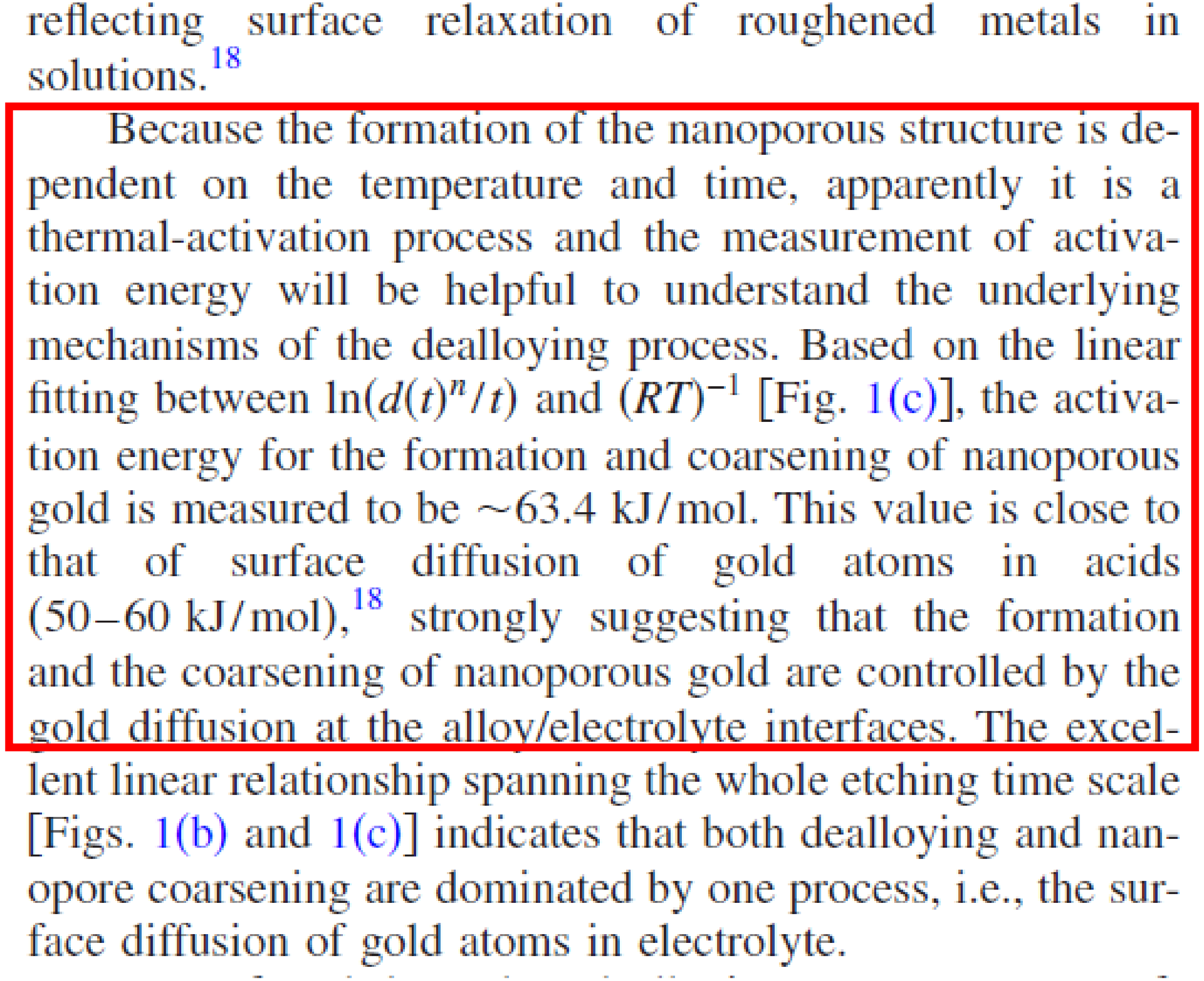

reflecting surface relaxation of roughened metals in solutions.[18]

Because the formation of the nanoporous structure is dependent on the temperature and time, apparently it is a thermal-activation process and the measurement of activation energy will be helpful to understand the underlying mechanisms of the dealloying process. Based on the linear fitting between $\ln(d(t)^n/t)$ and $(RT)^{-1}$ [Fig. 1(c)], the activation energy for the formation and coarsening of nanoporous gold is measured to be ~63.4 kJ/mol. This value is close to that of surface diffusion of gold atoms in acids (50–60 kJ/mol),[18] strongly suggesting that the formation and the coarsening of nanoporous gold are controlled by the gold diffusion at the alloy/electrolyte interfaces. The excellent linear relationship spanning the whole etching time scale [Figs. 1(b) and 1(c)] indicates that both dealloying and nanopore coarsening are dominated by one process, i.e., the surface diffusion of gold atoms in electrolyte.

63.4 kJ/mole=0.66 eV/at

Control of parameters by post-dealloying processes (annealings)

Applied Surface Science 355 (2015) 133–138

Contents lists available at ScienceDirect

Applied Surface Science

journal homepage: www.elsevier.com/locate/apsusc

Effect of annealing atmosphere on the thermal coarsening of nanoporous gold films

A.Y. Chen[a], S.S. Shi[a], F. Liu[a], Y. Wang[b], X. Li[a], J.F. Gu[c], X.F. Xie[d,*]

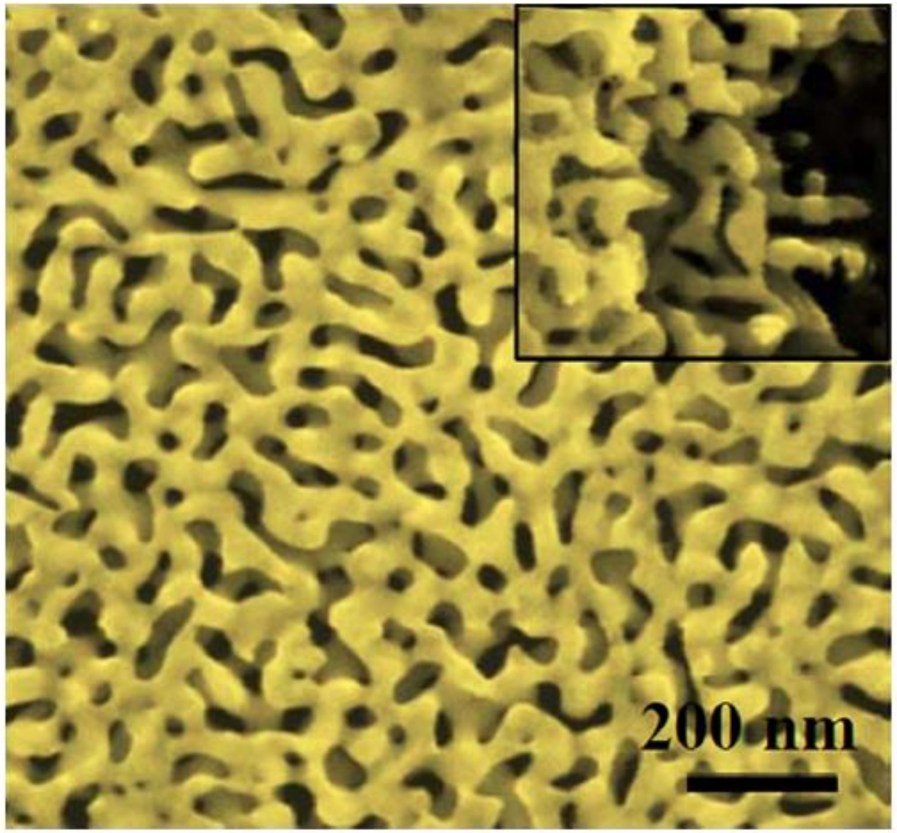

Fig. 1. SEM image of the as-prepared NPG film. The inset is the cross-sectional SEM morphology with the same scale bar.

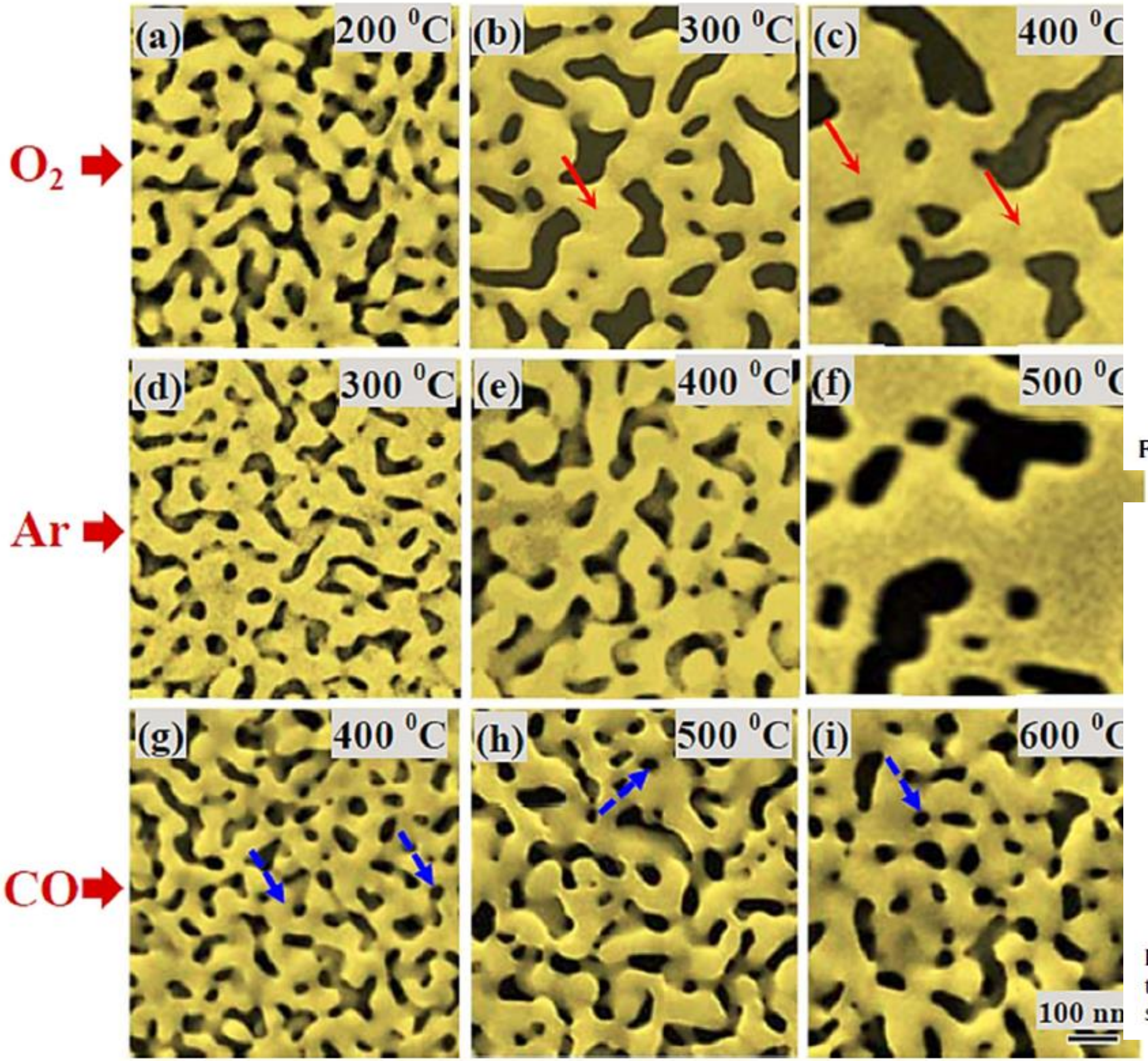

Fig. 2. SEM images of the NPG films annealed at different atmospheres for 2 h. (a–c) Annealed at 200, 300, and 400 °C in O_2, respectively; (d–f) annealed at 300, 400, and 500 °C in Ar, respectively; (g–i) annealed at 400, 500, and 600 °C in CO, respectively. All SEM images have the same scale bar.

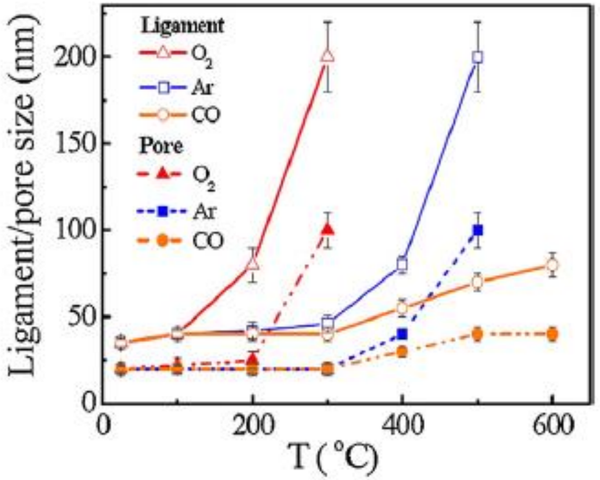

Fig. 3. Ligament and pore sizes of the NPG films annealed at different temperatures.

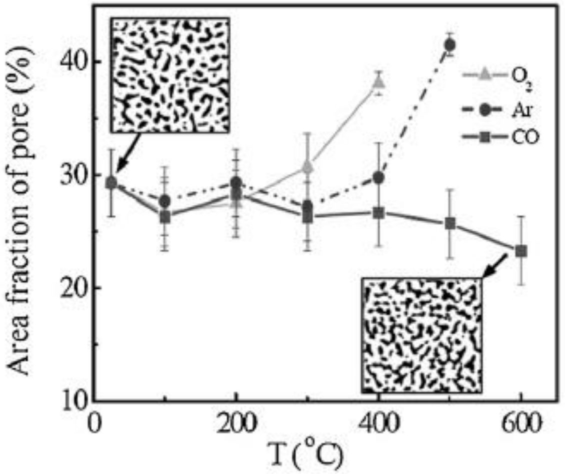

Fig. 5. Area fraction of the pore with dependence of temperature. The insets are the original NPG film (upper left) and that annealed in CO at 600 °C (lower right), showing the digital images for the estimation of porosity.

Post-dealloying annealings

Properties and Applications

- Plasmonic Properties (Optical Absorbance and Transmission measurements)
- SERS Detection for Analytes (Glyphosate, DNA,…..)
- Electrochemical Detection (Glucose,……)

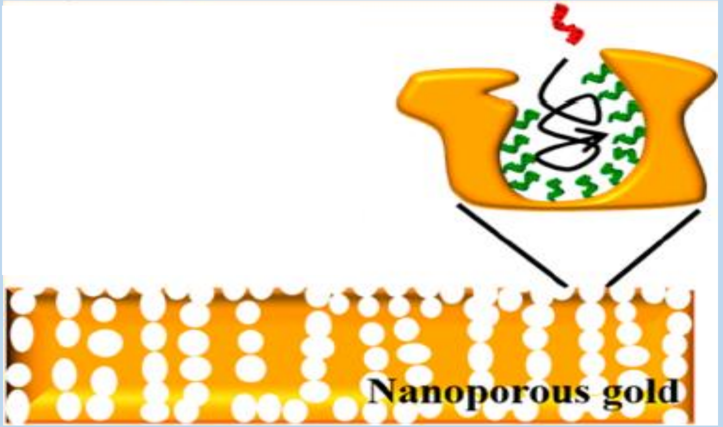

Nanoporous gold plasmonic structures for sensing applications

Received 29 Apr 2011; revised 1 Jun 2011; accepted 1 Jun 2011; published 22 Jun 2011
4 July 2011 / Vol. 19, No. 14 / OPTICS EXPRESS 13164

G. Ruffato,[1,2,3,*] F. Romanato,[1,2,3] D. Garoli,[1,2,3] and S. Cattarin[4]

[1]Department of Physics "G. Galilei," University of Padova, via Marzolo 8, 35131 Padova, Italy
[2]LaNN Laboratory for Nanofabrication of Nanodevices, VenetoNanotech, Corso Stati Uniti 4, 35127 Padova, Italy
[3]Institute for Materials Manufacturing (IOM-CNR), Area-Science Park, Basovizza 34012, Trieste, Italy
[4]Institute for Energetics and Interphases (IENI-CNR), Corso Stati Uniti 4, 35127 Padova, Italy
**gianluca.ruffato@unipd.it*

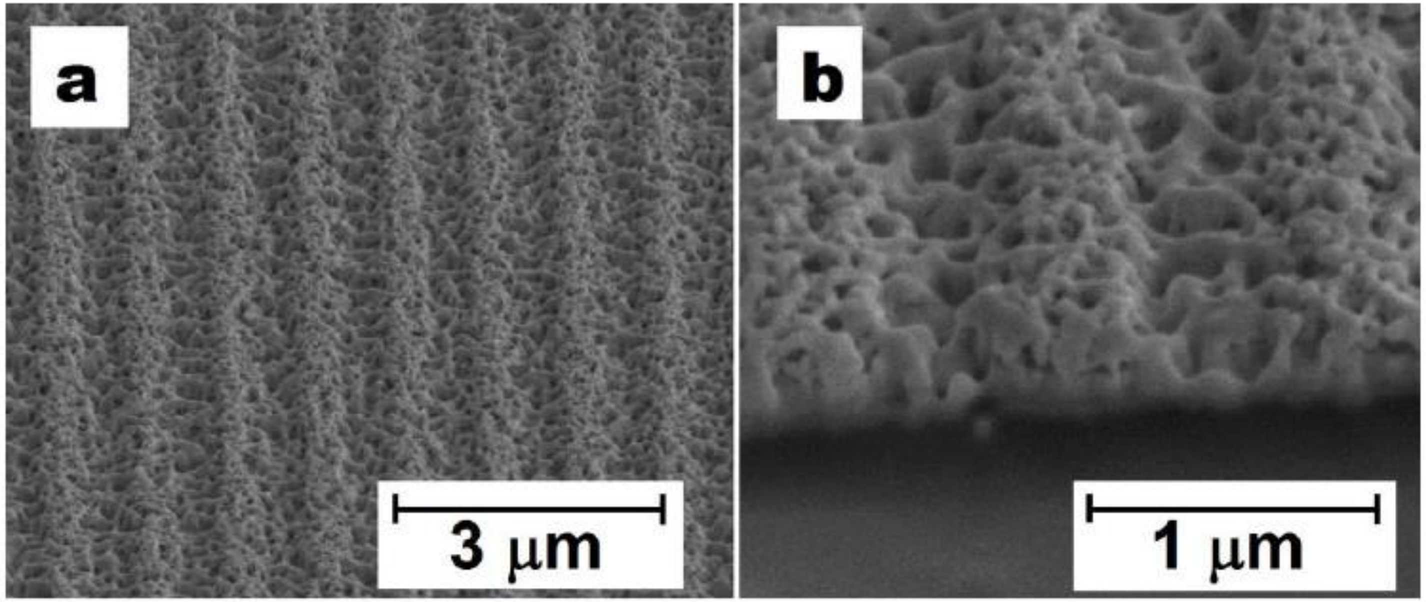

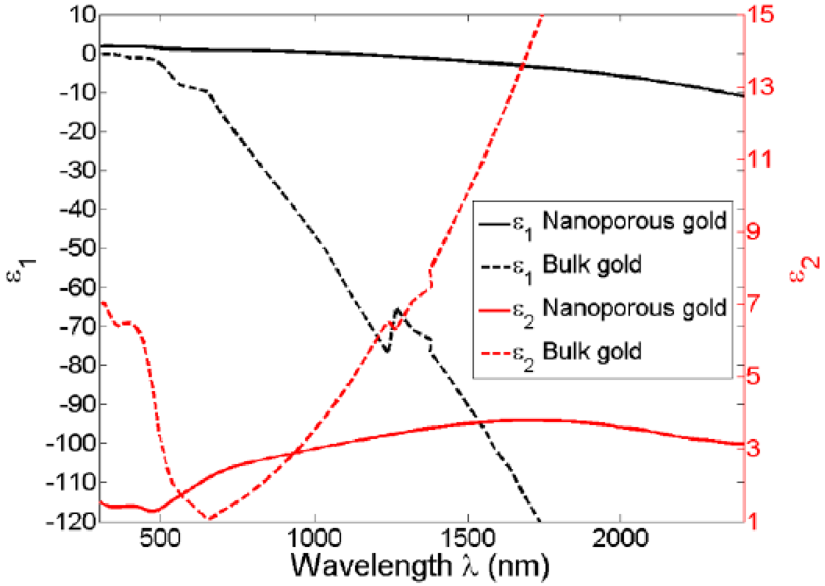

Fig. 2. Dielectric permittivity of nanoporous gold. Comparison with tabulated buk gold values.

APPLIED PHYSICS LETTERS **90**, 153120 (2007)

Surface enhanced Raman scattering of nanoporous gold: Smaller pore sizes stronger enhancements

L. H. Qian, X. Q. Yan, T. Fujita, A. Inoue, and M. W. Chen[a)]
International Frontier Center for Advanced Materials, Institute for Materials Research, Tohoku University, Sendai 980-8577, Japan

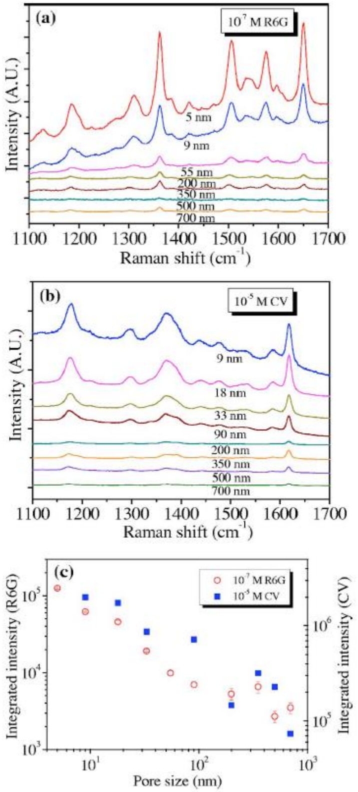

FIG. 2. (Color online) SERS spectra of nanoporous gold with different pore sizes for (a) 10^{-7} mol/l R6G aqueous solution and (b) 10^{-5} mol/l CV methanol solution. (c) Pore size dependence of the integrated intensities of 1650 cm^{-1} Raman band at the concentrations of 1×10^{-7} mol/l R6G and 1175 cm^{-1} Raman band at the concentrations of 1×10^{-5} mol/l CV. Laser excitation: 514.5 nm for R6G and 632.8 nm for CV.

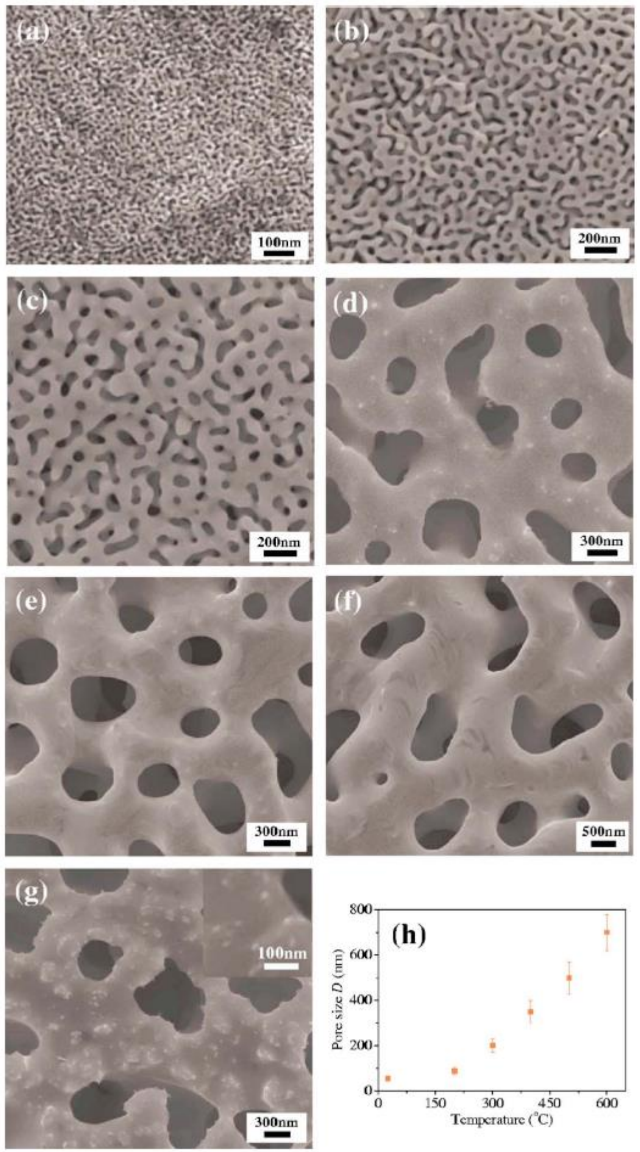

FIG. 1. (Color online) Representative SEM micrographs of nanoporous gold with various nanopore sizes. (a) Nanoporous gold film after 5 min dealloying at room temperature; (b) dealloyed at room temperature for 48 h; (c) thoroughly rinsed nanoporous gold annealed at 200 °C for 2 h; (d) 400 °C for 2 h; (e) 500 °C for 2 h, and (f) 600 °C for 2 h. (g) Nanoporous gold with short-time rinsing and annealed at 600 °C for 2 h. (h) The relationship between nanopore sizes (*D*) of thoroughly rinsed nanoporous gold and the annealing temperatures.

APPLIED PHYSICS LETTERS **92**, 251902 (2008)

Three-dimensional morphology of nanoporous gold

Takeshi Fujita,[1] Li-Hua Qian,[1] Koji Inoke,[2] Jonah Erlebacher,[3] and Ming-Wei Chen[1,a)]
[1]*WPI Advanced Institute for Materials Research, Tohoku University, Sendai 980-8577, Japan*
[2]*FEI Company Japan Ltd., Minato-ku, Tokyo 108-0075, Japan*
[3]*Department of Materials Science and Engineering, Johns Hopkins University, Maryland 21218, USA*

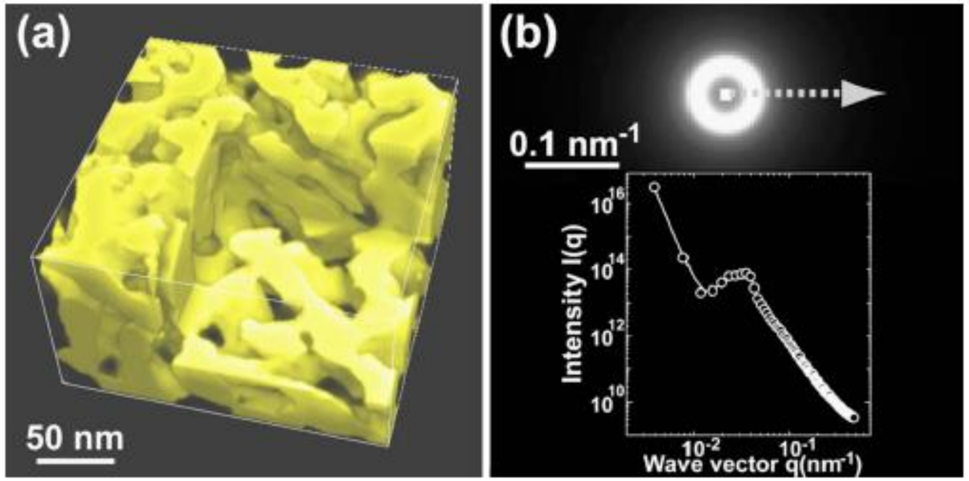

FIG. 2. (Color online) 3D tomographic reconstruction of nanoporous gold. (a) Magnified 3D image revealing the internal bicontinuous structure of nanoporous gold. (b) Fourier-transformed pattern showing the quasiperiodic feature of nanoporous gold. The inserted intensity profile was taken along the dash arrowhead in the Fourier-transform pattern.

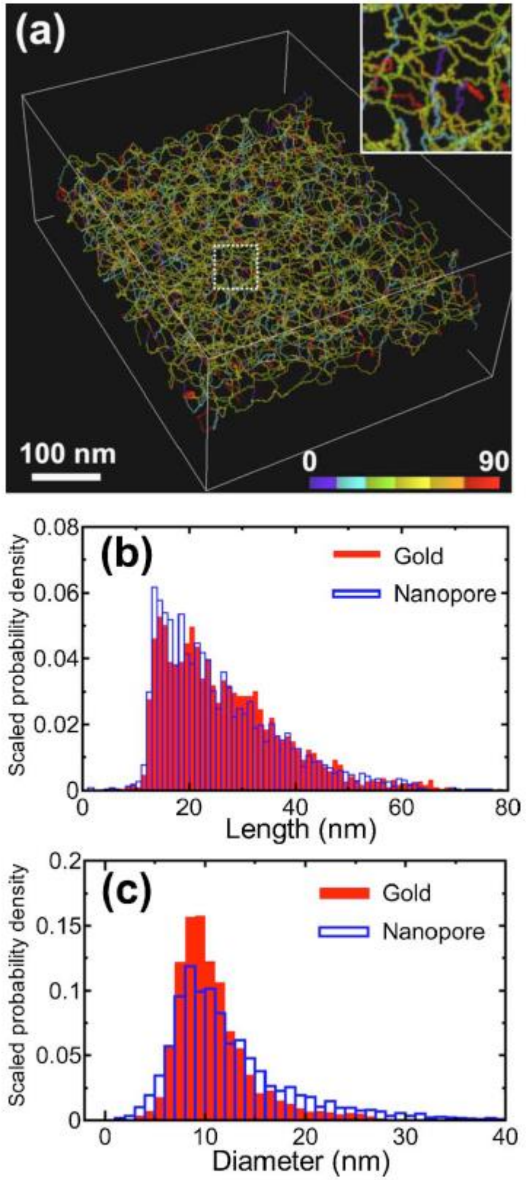

FIG. 3. (Color online) Quantitative length scale measurements. (a) Skeletal network of gold ligaments generated by using a 3D thinning algorithm. The insert shows a zoom-in image of the skeletal network with structural details. (b) Histograms of scaled probability density of interjunction path length of gold ligaments and nanopore channels. (c) Histograms of scaled probability density of the diameters of gold ligaments and nanopore channels. Both distributions prove that gold ligaments and nanopore channels are topologically equivalent.

APPLIED PHYSICS LETTERS **94**, 213109 (2009)

Geometric effect on surface enhanced Raman scattering of nanoporous gold: Improving Raman scattering by tailoring ligament and nanopore ratios

X. Y. Lang, L. Y. Chen, P. F. Guan, T. Fujita, and M. W. Chen[a)]
WPI Advanced Institute for Materials Research, Tohoku University, Sendai 980-8577, Japan

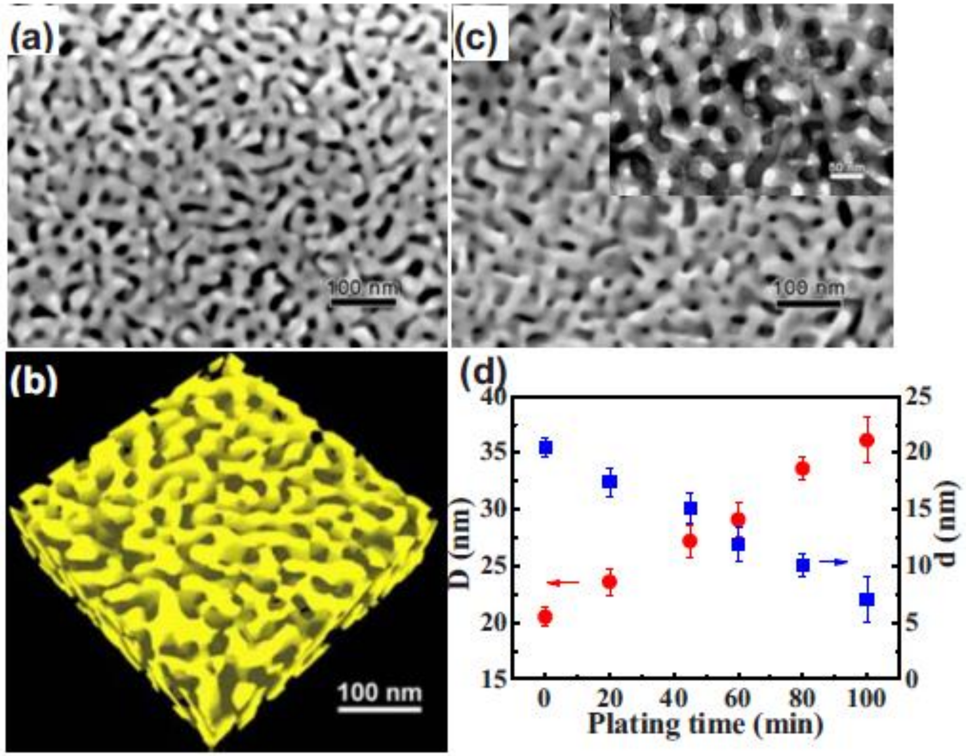

FIG. 1. (Color online) Representative (a) top-view SEM micrograph and (b) 3D electron tomigraphic image of the AP-NPG films with $d \approx D \approx 20.5$ nm. (c) Top-view SEM of the GP-NPG films Au plated for 100 min. Inset: TEM micrograph. (d) Relationship between t and D or d of GP-NPG films.

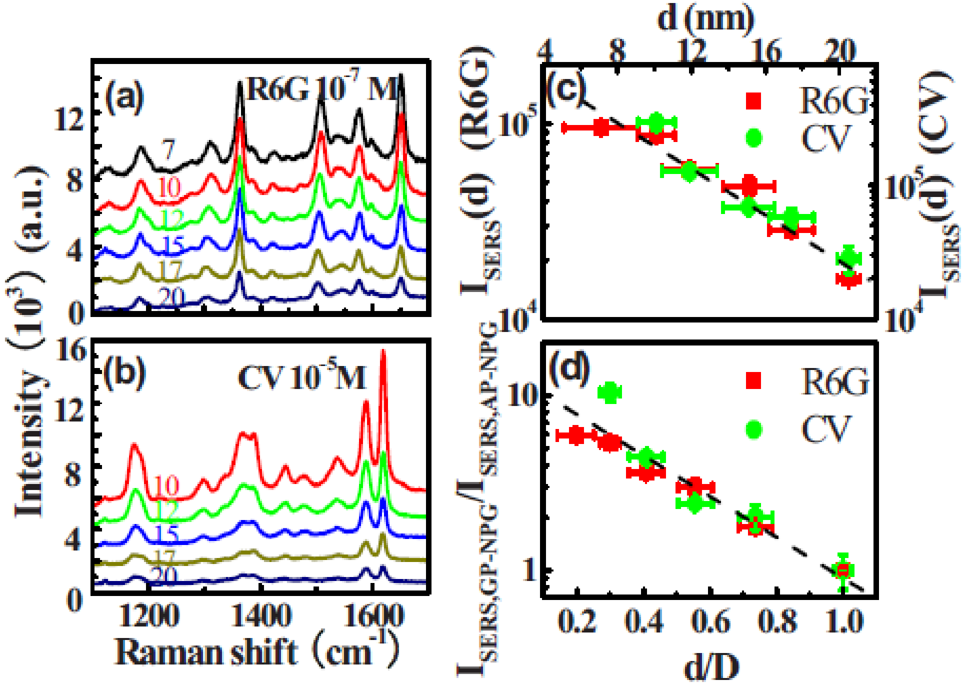

FIG. 2. (Color online) SERS spectra of (a) R6G and (b) CV molecules adsorbed on GP-NPG films with different d/D ratios. Laser excitation: 514.5 nm for both molecules. (c) Nanopore-size dependence of the integrated SERS intensity of Raman bands of R6G and CV at 1650 and 1175 cm^{-1}, respectively. (d) The normalized SERS enhancements of GP-NPG films ($I_{SERS,GP\text{-}NPG}/I_{SERS,AP\text{-}NPG}$) as a function of the d/D ratios.

APPLIED PHYSICS LETTERS **98**, 093701 (2011)

Localized surface plasmon resonance of nanoporous gold

Xingyou Lang,[1] Lihua Qian,[1] Pengfei Guan,[1] Jian Zi,[2] and Mingwei Chen[1,a)]
[1]*WPI Advanced Institute for Materials Research, Tohoku University, Sendai 980-8577, Japan*
[2]*Department of Physics, Surface Physics Laboratory, Fudan University, Shanghai 200433, China*

(Received 18 November 2010; accepted 10 February 2011; published online 28 February 2011)

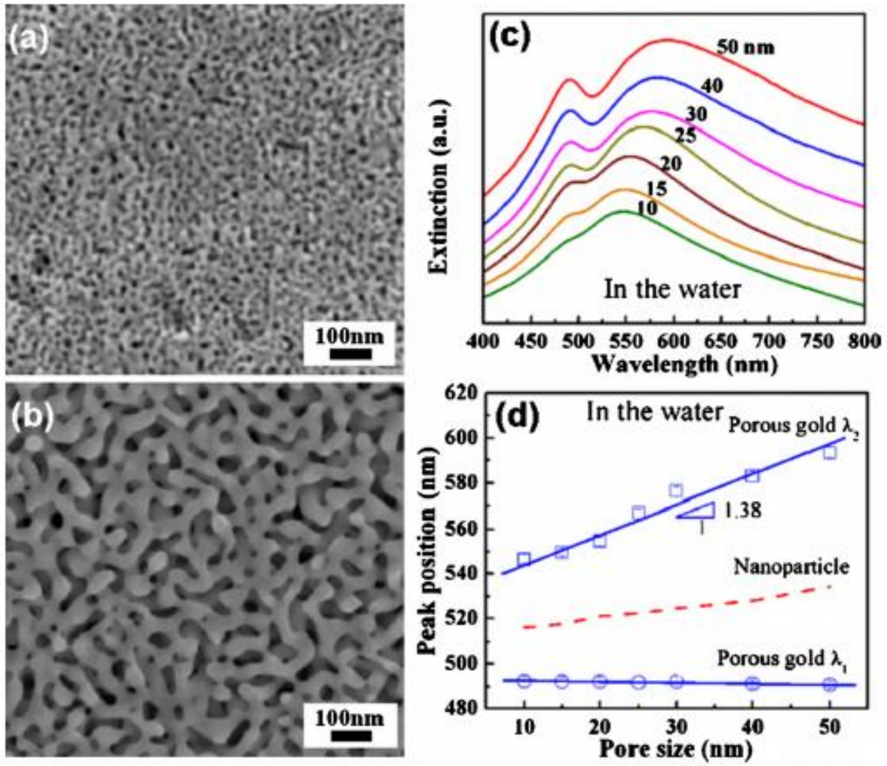

FIG. 1. (Color online) SEM micrographs of NPG synthesized by means of free corrosion for 5 min (a) and 24 h (b). (c) UV-Vis extinction spectra and (d) the resonant peak position of λ_1 and λ_2 of NPG with the pore sizes of 10–50 nm in water. For comparison, the dashed line represents the size dependence resonant band of gold nanoparticles.

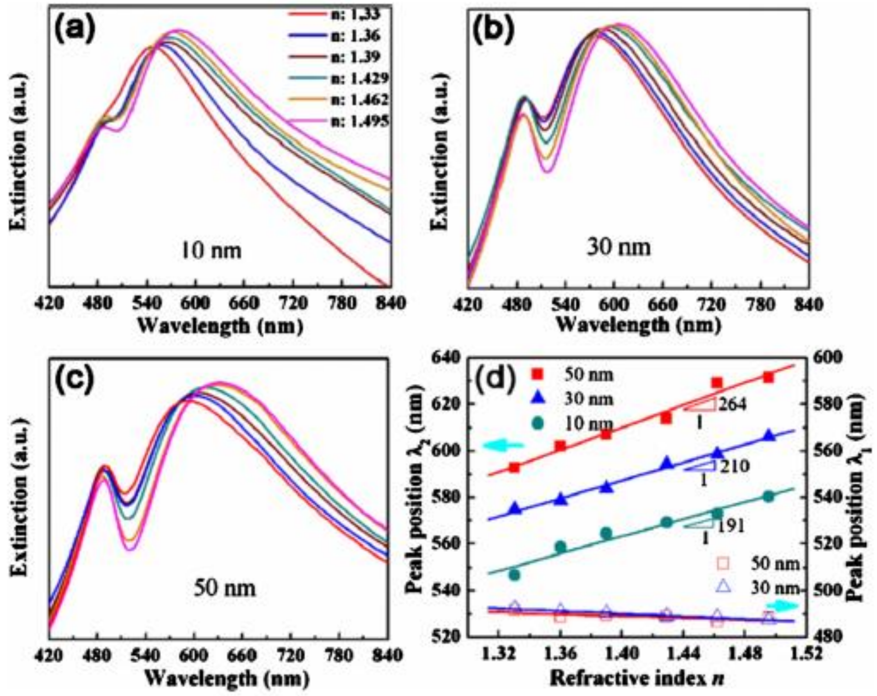

FIG. 2. (Color online) UV-Vis extinction spectra of porous gold films with (a) 10 nm; (b) 30 nm, and (c) 50 nm are recorded by immersing them into various dielectric environments. Refractive index of these solution increases from left to right: water (n=1.33), ethanol (n=1.36), 3:1 ethanol/toluene (n=1.39), 1:1 ethanol/toluene (n=1.429), 1:3 ethanol/toluene (n=1.462), and toluene (n=1.495). (d) Dependence of resonance (λ_1, empty symbols) and LSPR (λ_2, solid symbols) peaks of NPG films on refractive index.

APPLIED PHYSICS LETTERS **96**, 073701 (2010)

Size dependence of molecular fluorescence enhancement of nanoporous gold

X. Y. Lang,[a)] P. F. Guan, L. Zhang, T. Fujita, and M. W. Chen[a)]
WPI Research Center, Advanced Institute for Materials Research, Tohoku University,
Sendai 980-8577, Japan

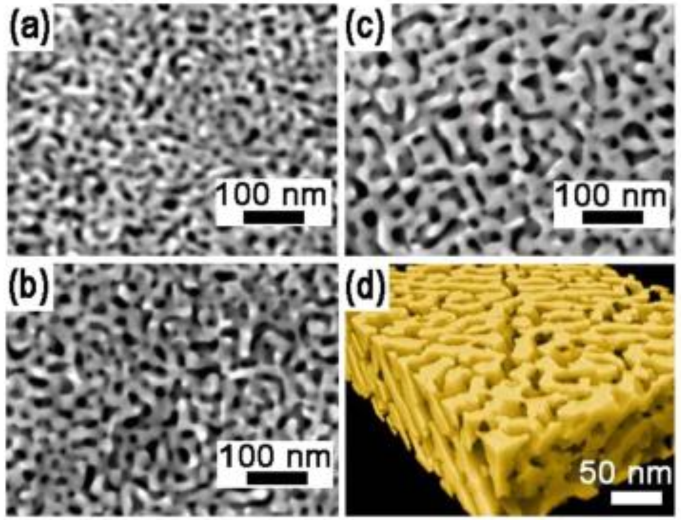

FIG. 1. (Color online) Top-view SEM micrograph of dealloyed $Ag_{65}Au_{35}$ with an average nanopore sizes of (a) 10, (b) 20, and (c) 30 nm. (d) Three-dimensional electron tomograph of NPG with the nanopore size of ~10 nm.

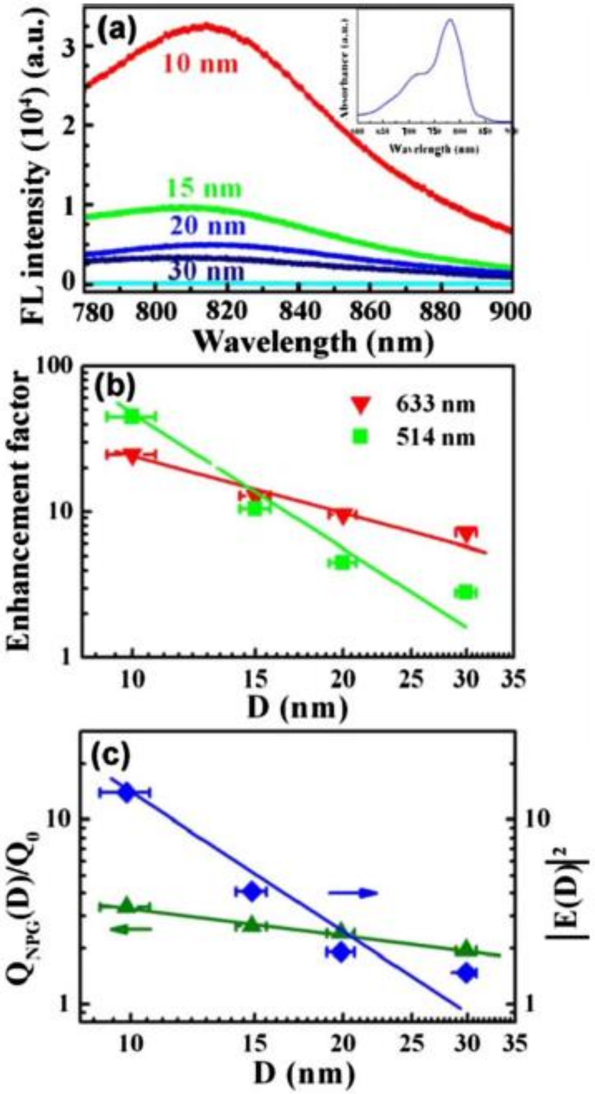

FIG. 2. (Color online) (a) Fluorescence emission spectra of ICG conjugated to the HSA-coated NPG films with different pore size (D). Inset: Absorption spectrum of ICG. (b) EFs of ICG/HSA/NPG films as a function of D under the excitations of 514.5 and 632.8 nm, respectively. (c) Pore size dependence of near-field ($|E(D)|^2$) and quantum yield enhancements ($Q_{NPG}(D)/Q_0$) of ICG/HSA/NPG films under the illumination of 514.5 nm.

PHYSICAL REVIEW B **78**, 165418 (2008)

Percolation in nanoporous gold and the principle of universality for two-dimensional to hyperdimensional networks

G. B. Smith, A. I. Maaroof, and M. B. Cortie
Department of Physics and Advanced Materials and Institute for Nanoscale Technology, University of Technology, Sydney, P.O. Box 123, Broadway, New South Wales 2007, Australia

(Received 10 April 2008; revised manuscript received 5 September 2008; published 22 October 2008)

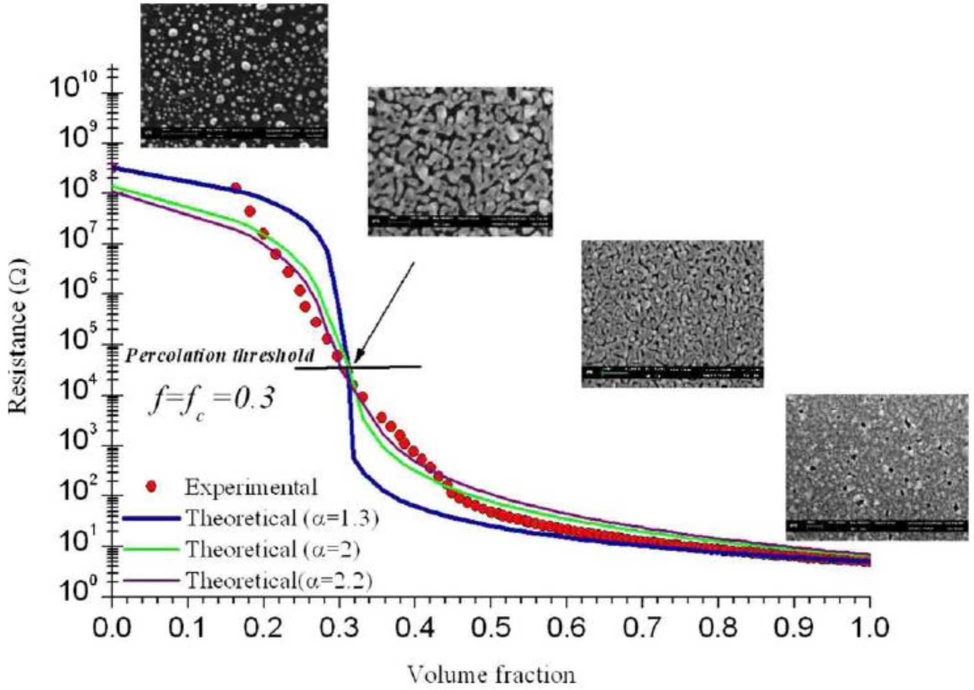

FIG. 3. (Color online) Resistance of a growing gold film on glass as a function of volume (or area) fraction f of gold. Images included show characteristic morphology at each stage of gold coverage. Models for $d=2$ and $d=3$ percolation are included, along with a critical curve for $\alpha=2.2$.

ELSEVIER
Available online at www.sciencedirect.com
ScienceDirect
Scripta Materialia 65 (2011) 17–20
Scripta MATERIALIA
www.elsevier.com/locate/scriptamat

Nanoporous gold for enzyme-free electrochemical glucose sensors

L.Y. Chen, X.Y. Lang, T. Fujita and M.W. Chen*

WPI Advanced Institute for Materials Research, Tohoku University, Sendai 980-8577, Japan

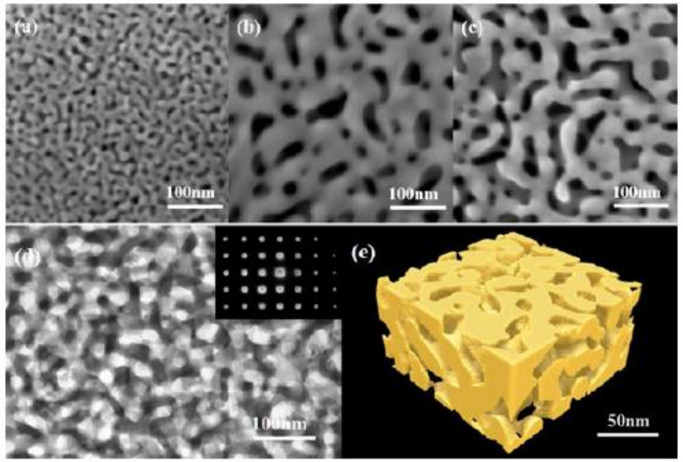

Figure 1. SEM and TEM images of NPG by dealloying $Au_{35}Ag_{65}$ in concentrated acid at room temperature. (a) SEM micrograph of NPG dealloyed for 15 min; (b) SEM micrograph of NPG dealloyed for 2 h; (c) SEM micrograph of NPG dealloyed for 4 h; (d) TEM micrograph of NPG dealloyed for 15 min; and (e) electron tomograph of the NPG dealloyed for 15 min. The inset in (d) shows the selected area electron diffraction pattern of NPG.

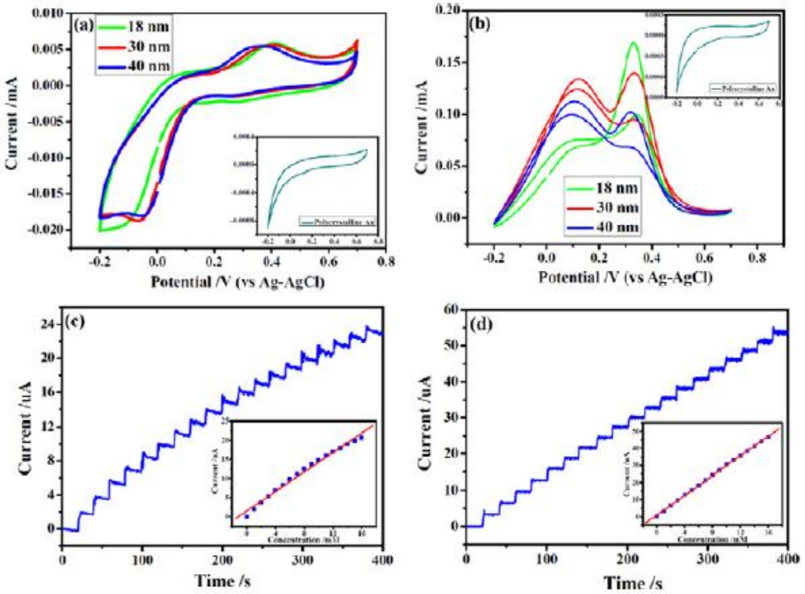

Figure 2. CV curves of NPG with different pore sizes and polycrystalline Au (insets) (a) in 0.1 M PBS and (b) in 0.1 M PBS containing 50 mM glucose. Scan rate: 50 mV s^{-1}. Chronoamperometry curves of NPG with pore size of 18 nm in 0.1 M PBS solution with successive addition of 1 mM glucose at the constant potentials of (c) 0.1 V and (d) 0.3 V, respectively.

analytical chemistry
Article
pubs.acs.org/ac

Effect of Nanoporous Gold Thin Film Morphology on Electrochemical DNA Sensing

Pallavi Daggumati, Zimple Matharu, and Erkin Seker*

Department of Electrical and Computer Engineering, University of California, Davis, Davis, California 95616, United States

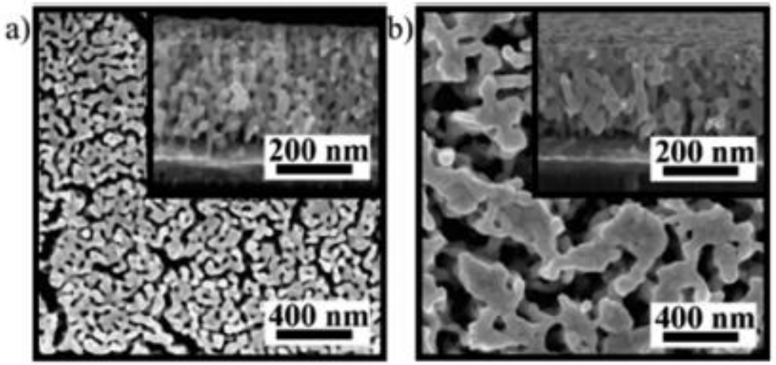

Figure 1. Scanning electron microscope images of (a) unannealed np-Au film; (b) annealed np-Au film (obtained via thermal treatment at 225 °C). Insets: cross-sectional views.

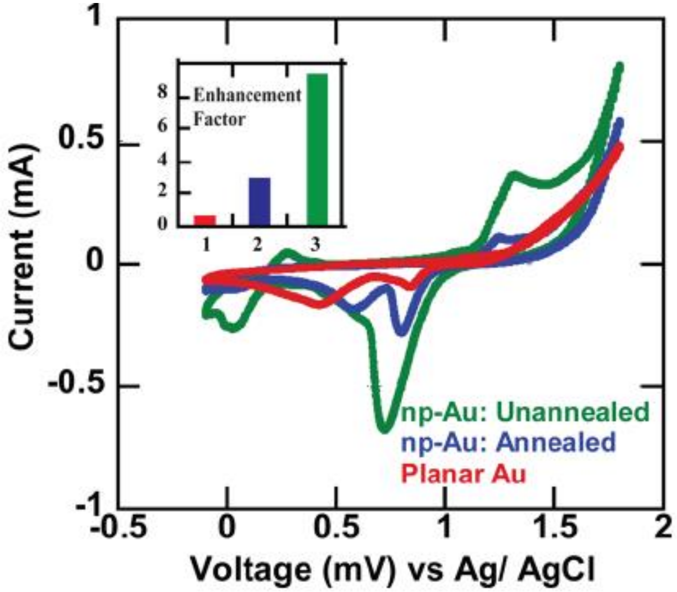

Figure 2. CV measurements of np-Au, annealed np-Au, and planar Au films performed in 0.05 M sulfuric acid at a scan rate of 50 mV/s. Inset: enhancement factors of different morphologies: (1) planar Au, (2) annealed np-Au, and (3) unannealed np-Au.

Scheme 1. Hybridization Event in Unannealed and Annealed np-Au Morphologies[a]

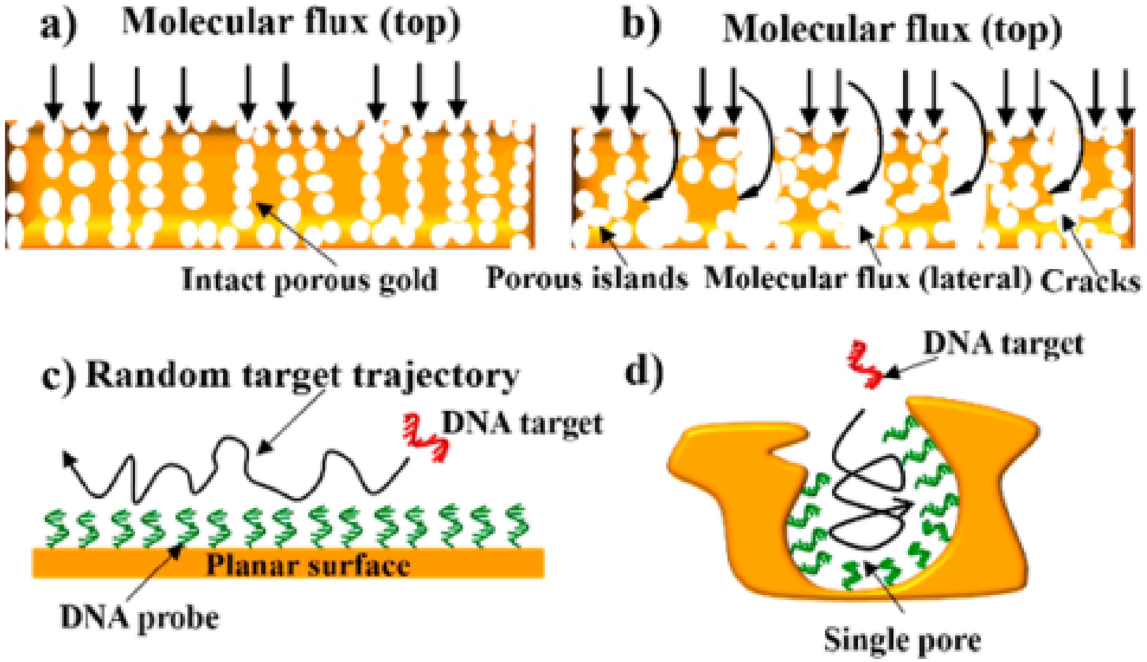

[a](a) For the unannealed np-Au with minimal cracks, the molecules (e.g., DNA probes) can permeate the porous films only from the top surface. (b) For annealed np-Au with cracks separating the porous islands, the molecules can permeate the porous film from the top and side of the islands, thereby enhancing the accessibility of the porous electrode. (c) For a planar electrode, a target DNA moving randomly through the solution has a small probability of making molecular contact, that is, hybridizing with the immobilized DNA probes. (d) For a porous electrode, once the target DNA enters the pore, it is surrounded by surfaces immobilized with probe DNA and the random movement yields a much higher hybridization probability.

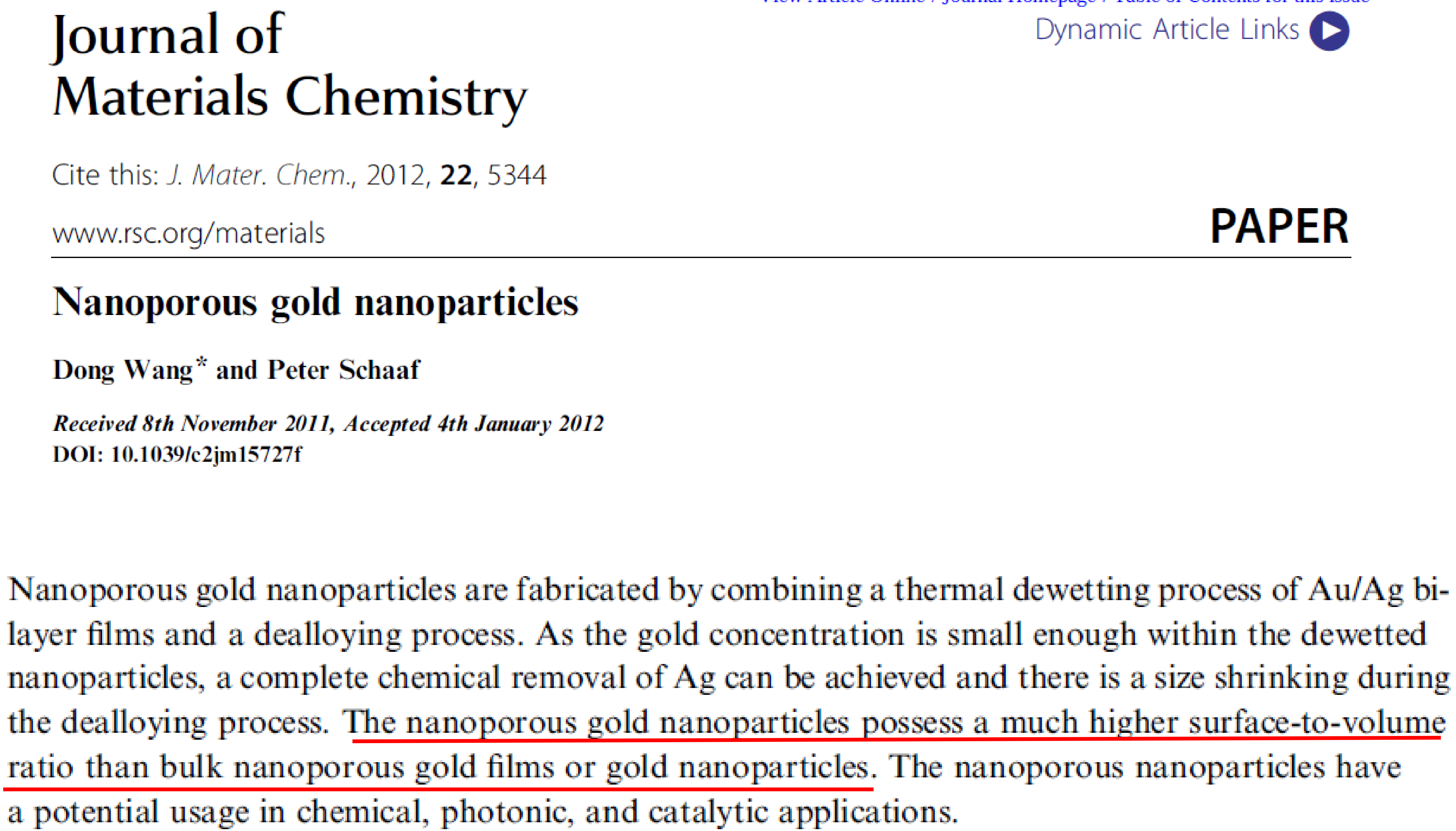

Journal of
Materials Chemistry

Cite this: *J. Mater. Chem.*, 2012, **22**, 5344

www.rsc.org/materials

PAPER

Nanoporous gold nanoparticles

Dong Wang* and Peter Schaaf

Received 8th November 2011, Accepted 4th January 2012
DOI: 10.1039/c2jm15727f

Nanoporous gold nanoparticles are fabricated by combining a thermal dewetting process of Au/Ag bi-layer films and a dealloying process. As the gold concentration is small enough within the dewetted nanoparticles, a complete chemical removal of Ag can be achieved and there is a size shrinking during the dealloying process. The nanoporous gold nanoparticles possess a much higher surface-to-volume ratio than bulk nanoporous gold films or gold nanoparticles. The nanoporous nanoparticles have a potential usage in chemical, photonic, and catalytic applications.

Au/Ag bi-layer films with different layer thicknesses (5 nm Au/20 nm Ag and 10 nm Au/20 nm Ag) were deposited on SiO_2/Si substrates using electron beam evaporation. 200 nm thermal SiO_2 were grown on the Si substrates prior to deposition in order to prevent the reaction between the substrate and the subsequently deposited films. The dewetting of the bi-layer films was induced by annealing at 900 °C in Ar for 15 min. After annealing, the samples were submerged in a 65 wt% HNO_3 aqueous solution at 21 °C for 5 min. The dewetted nanoparticles and the nano-

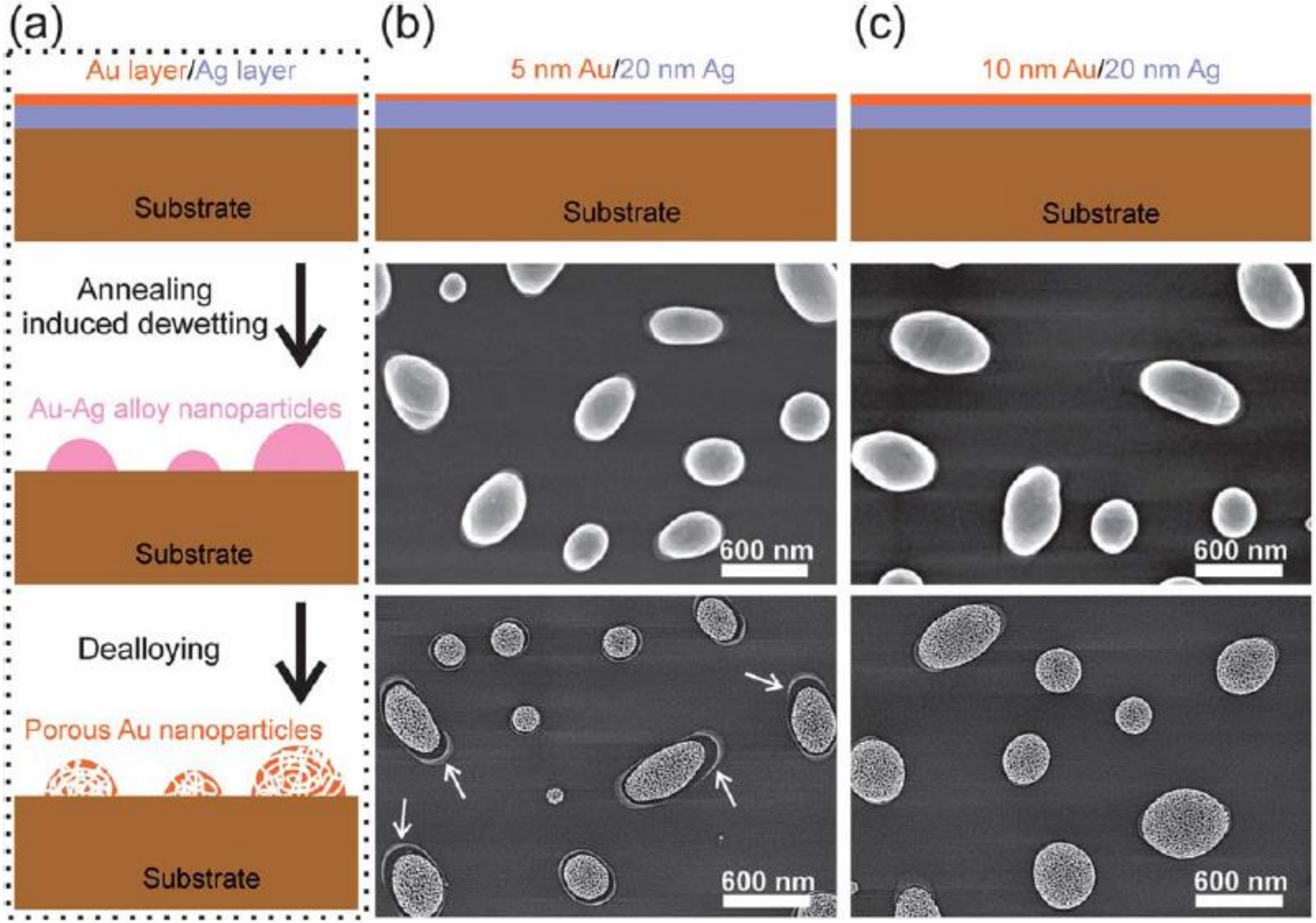

Fig. 1 (a) Schematic drawing of the synthesis of nanoporous gold nanoparticles by combining the dewetting process (for alloy nanoparticles) and the dealloying process (for nanoporous gold). (b) Schematic drawing of the 5 nm Au/20 nm Ag films (upper panel) and the corresponding SEM images of the dewetted alloy nanoparticles (middle panel) and formed nanoporous gold nanoparticles (lower panel). White arrows in the lower panel SEM image indicate the contour of the particles before dealloying. (c) Schematic drawing of the 10 nm Au/20 nm Ag films (upper panel) and the corresponding SEM images of the dewetted alloy nanoparticles (middle panel) and formed nanoporous gold particles (lower panel).

quently deposited metal films and the Si substrate. Au/Ag bilayers with different layer thicknesses (10 nm/20 nm, 10 nm/25 nm, 10 nm/30 nm, 15 nm/25 nm, and 15 nm/30 nm) were deposited onto the prepatterned substrates by e-beam evaporation, and then annealed at 700 °C in Ar for 15 min to induce dewetting. This temperature is well below the solidus temperature of the Au–Ag system, i.e., the dewetting is solid-state dewetting. Hence, interdiffusion of Au and Ag occurred, and perfectly ordered arrays of Au–Ag alloy nanoparticles were formed on the prepatterned substrates. Subsequently, de-

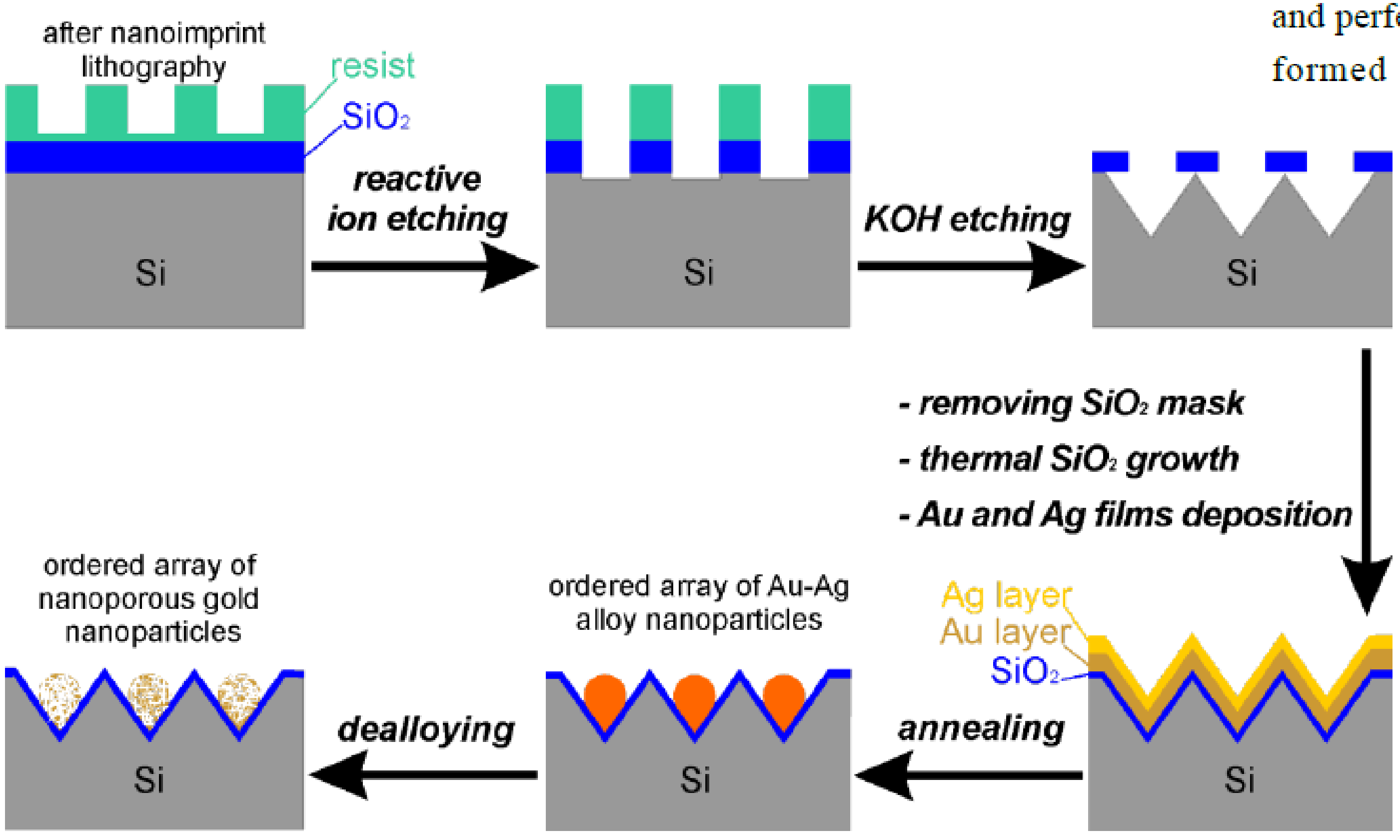

Figure 1: Schematics of the fabrication process for an ordered array of nanoporous gold nanoparticles.

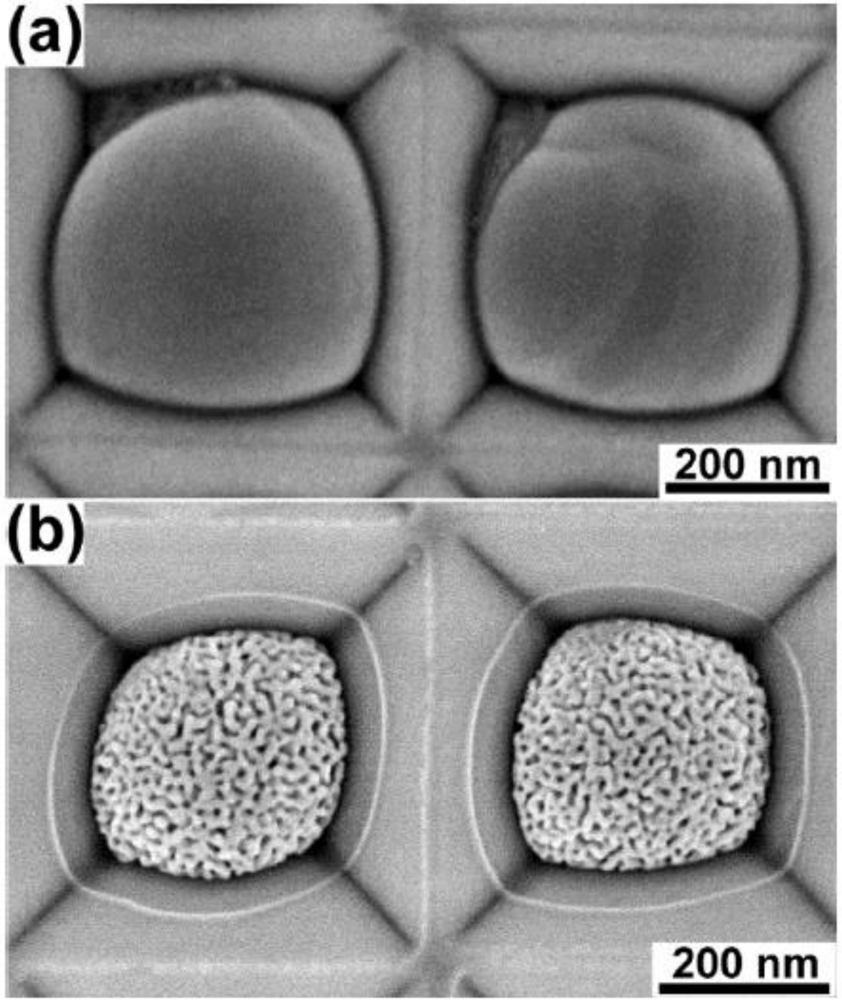

Figure 2: SEM micrographs of samples before and after dealloying: (a) ordered array of Au–Ag alloy nanoparticles dewetted from the 15 nm Au/30 nm Ag bilayers, and (b) ordered array of nanoporous gold nanoparticles formed after the subsequent dealloying.

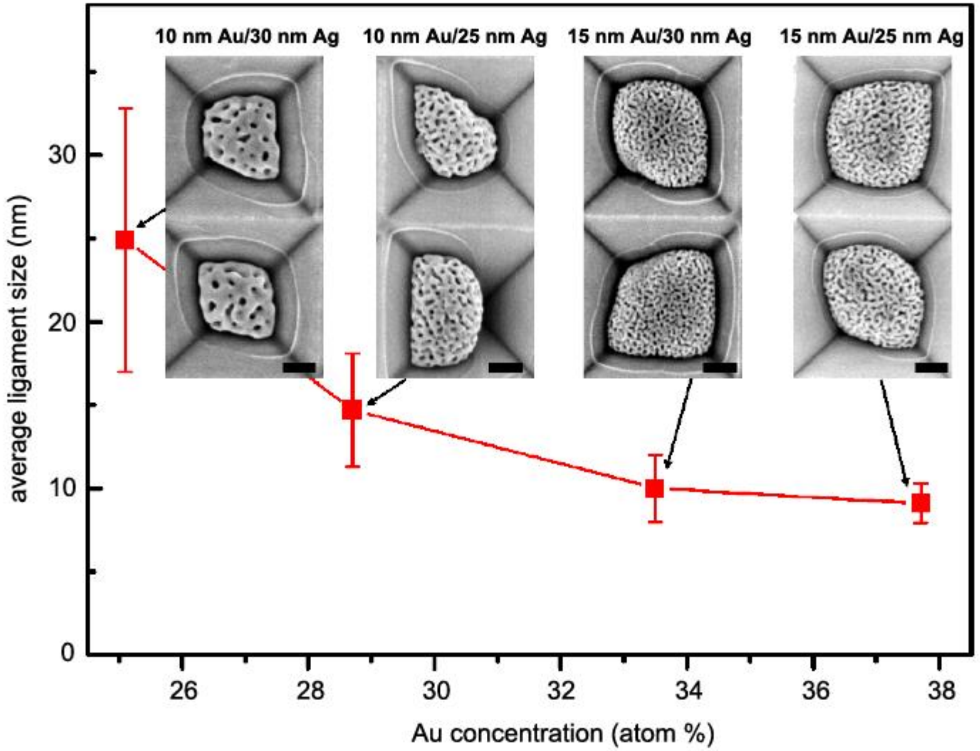

Figure 4: Plot of the average ligament size as a function of the Au concentration of alloy nanoparticles. The error bars represent the standard deviation. Insets show the corresponding SEM images. Scale bars in the insets are 100 nm.

Nanoporous Au Particles

Aim of the present work

Comparison of the Characteristics (Porosity) of Nanoporous Au Particles Produced on Surfaces by Alloying and Dewetting of Au/Ag Nanoscale-Thick Bilayers in the

- **SOLID-STATE**

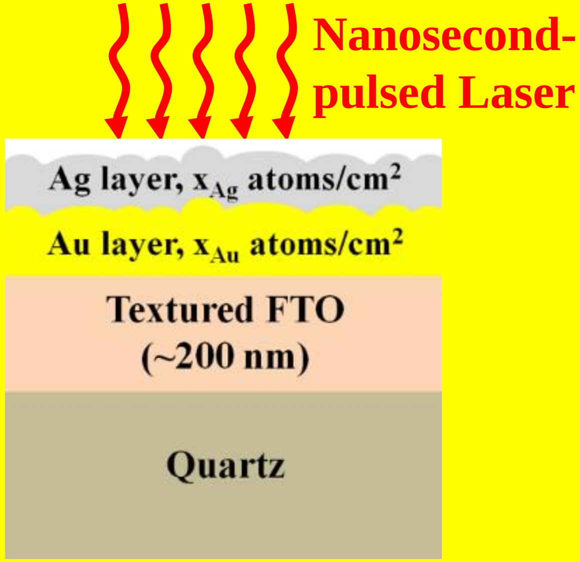

- **MOLTEN-STATE**

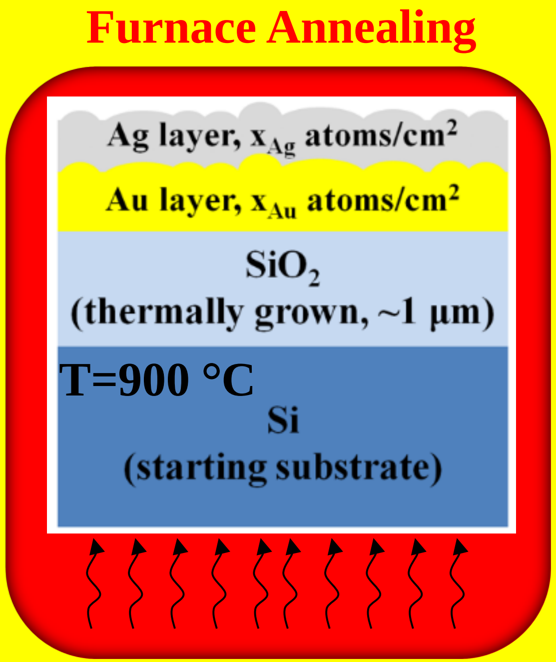

Samples Preparation and Characterization

Starting Substrates

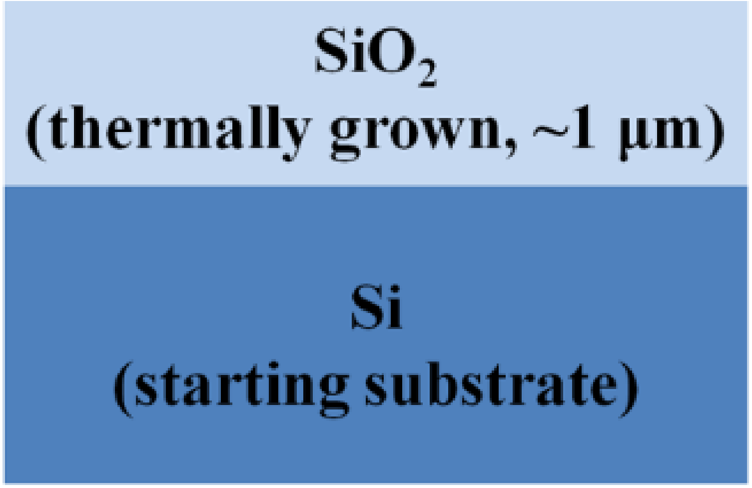

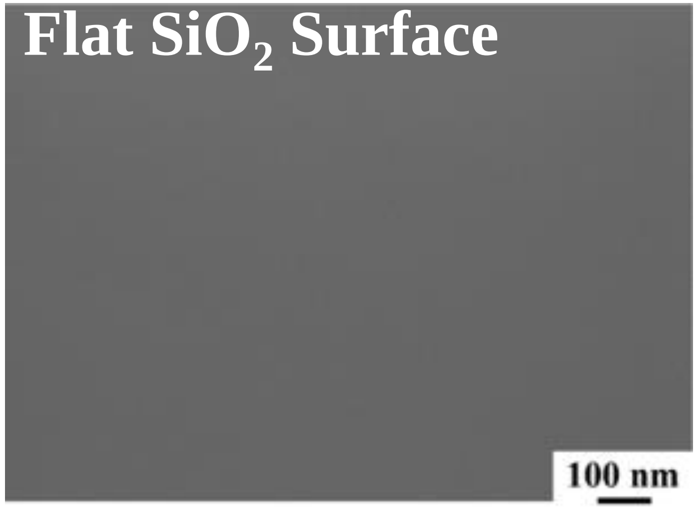
Flat SiO_2 Surface

F. Ruffino et al., J. Mater. Sci. 49, 8498 (2014)
F. Ruffino et al., Superlatt. Microstruct. 103, 28 (2017)

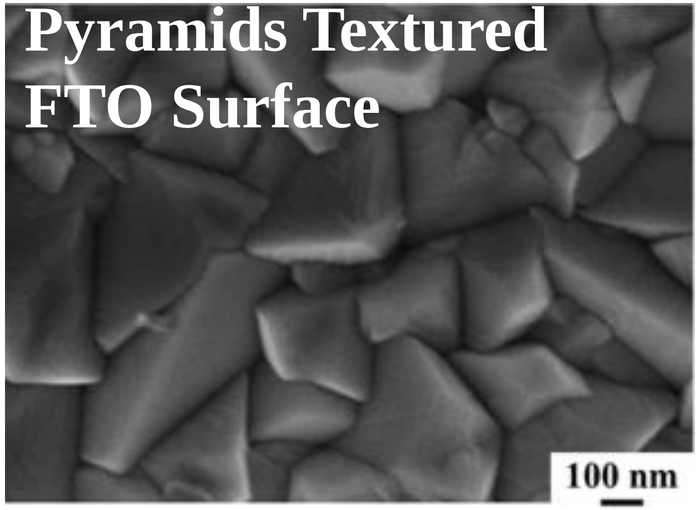
Pyramids Textured FTO Surface

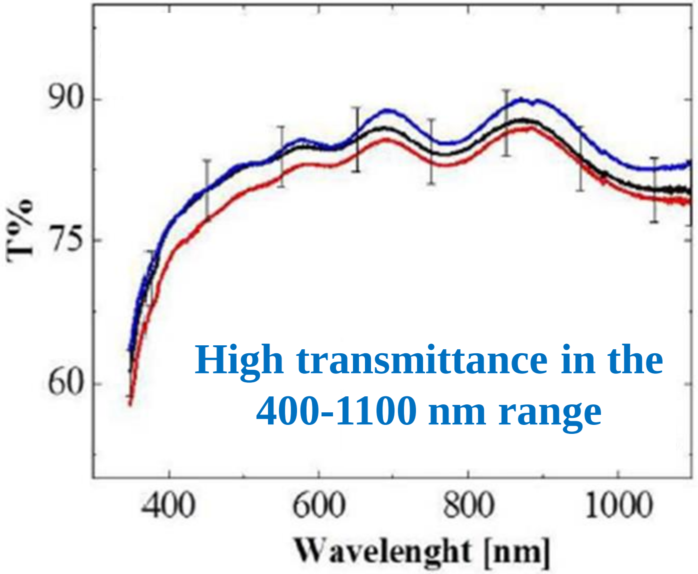

High transmittance in the 400-1100 nm range

Samples Preparation and Characterization

Au-Ag Bilayers Deposition (Sputtering)

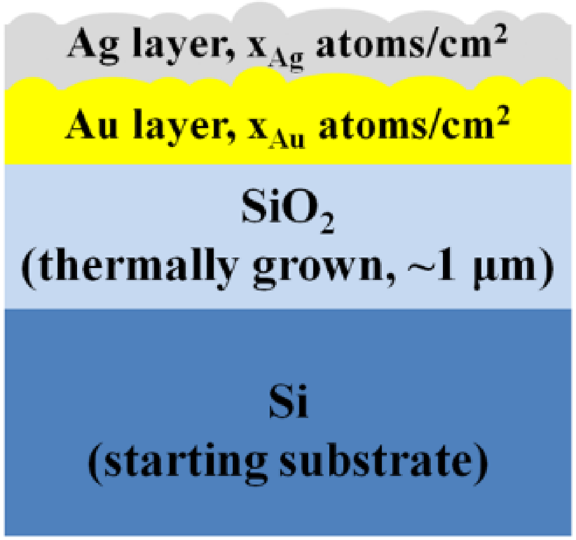

Ag layer, x_{Ag} atoms/cm^2

Au layer, x_{Au} atoms/cm^2

SiO_2
(thermally grown, ~1 μm)

Si
(starting substrate)

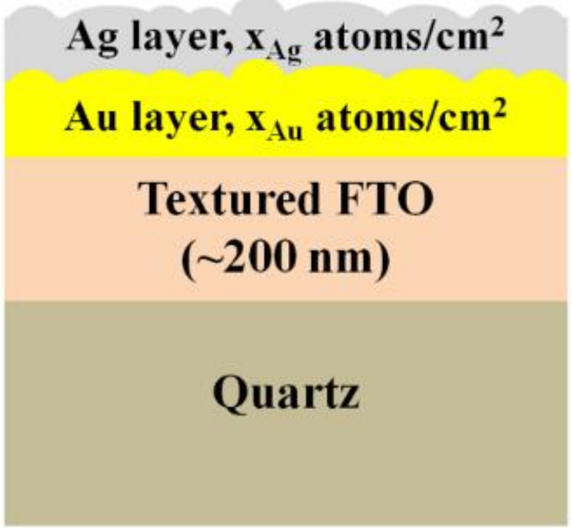

Ag layer, x_{Ag} atoms/cm^2

Au layer, x_{Au} atoms/cm^2

Textured FTO
(~200 nm)

Quartz

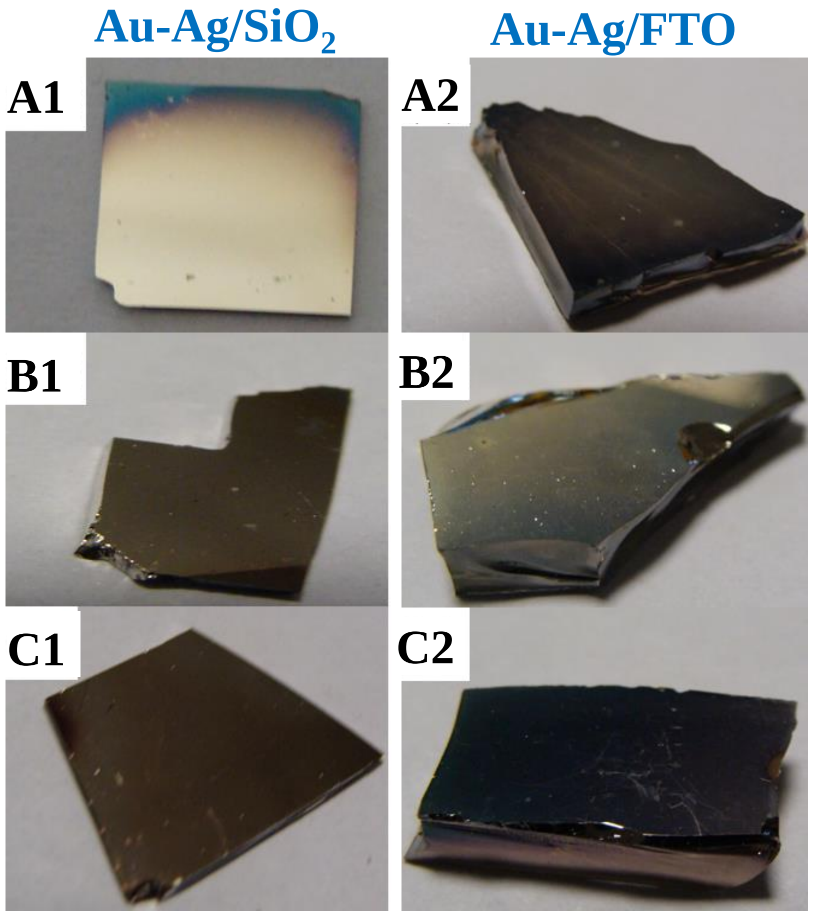

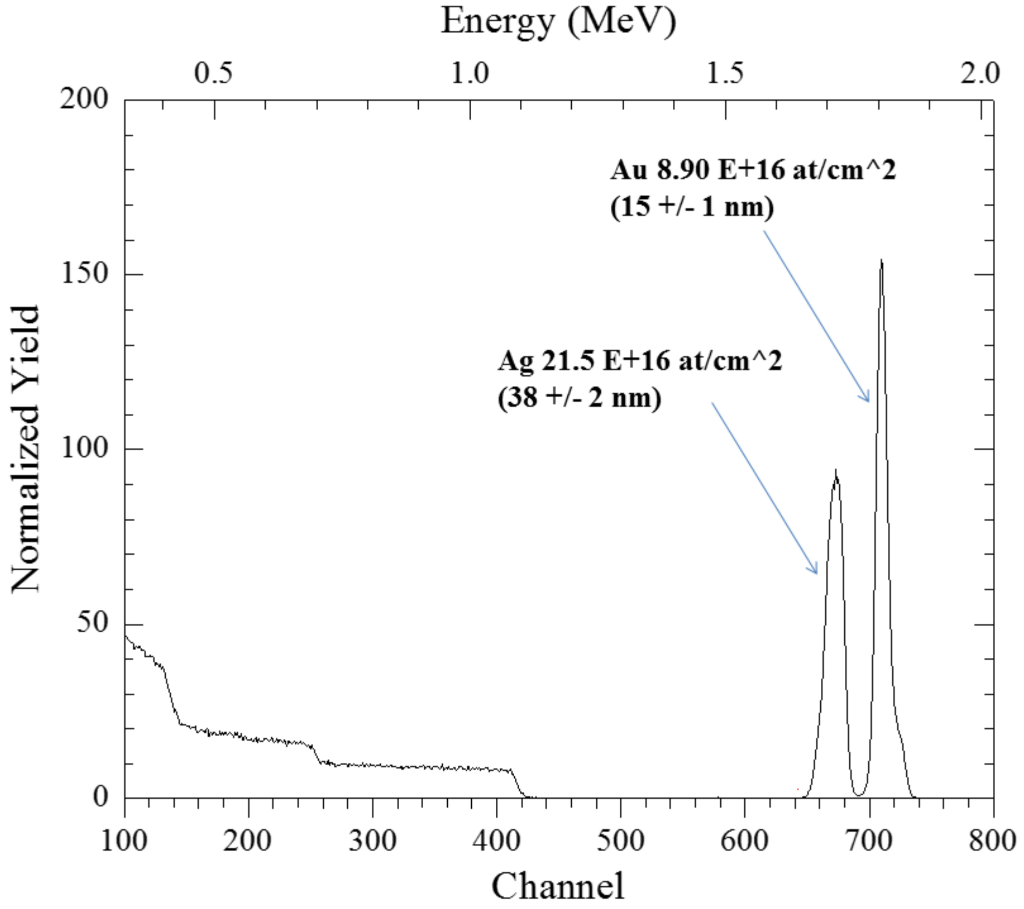

Au 8.90 E+16 at/cm^2
(15 +/- 1 nm)

Ag 21.5 E+16 at/cm^2
(38 +/- 2 nm)

Samples	Au/cm^2	Ag/cm^2	Au thickness (nm)	Ag thickness (nm)	Au at.%-Ag at. %
A1, A2	8.9×10^{16}	21.5×10^{16}	15.0 ± 1.0	38.0 ± 2.0	$Au_{29}Ag_{71}$
B1, B2	4.6×10^{16}	31.2×10^{16}	7.7 ± 0.5	50.0 ± 3.0	$Au_{13}Ag_{87}$
C1, C2	18.7×10^{16}	24.4×10^{16}	31.0 ± 2.0	41.0 ± 2.0	$Au_{44}Ag_{56}$

Samples Preparation and Characterization

Au-Ag Bilayers Deposition (Sputtering)

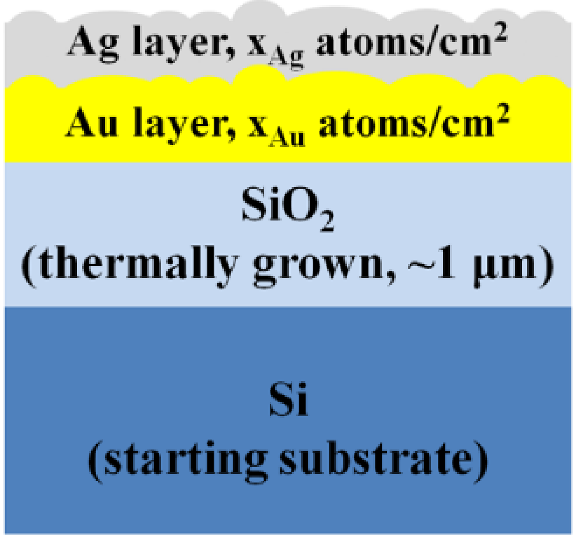
Ag layer, x_{Ag} atoms/cm^2

Au layer, x_{Au} atoms/cm^2

SiO_2
(thermally grown, ~1 µm)

Si
(starting substrate)

Au 15 nm-Ag 38 nm/SiO_2

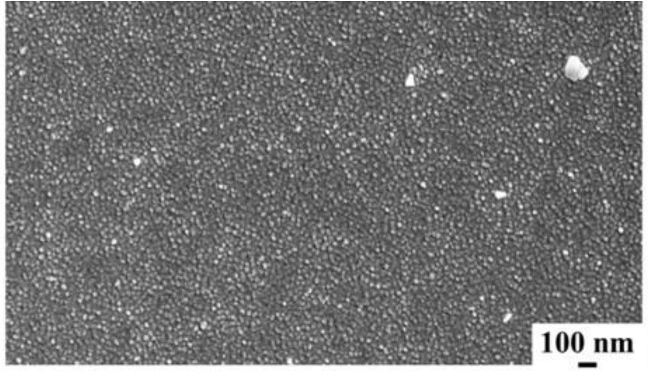

Au 7.7 nm-Ag 50 nm/SiO_2

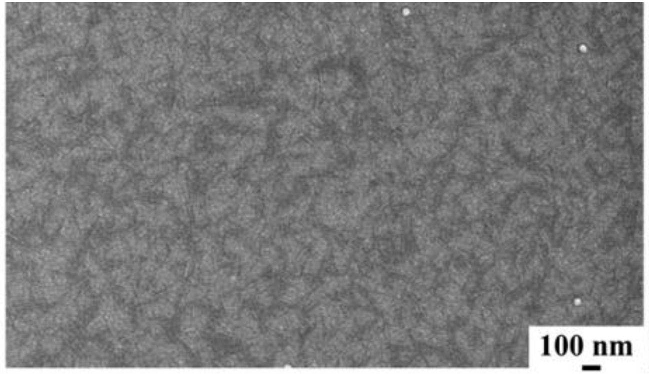

Au 31 nm-Ag 41 nm/SiO_2

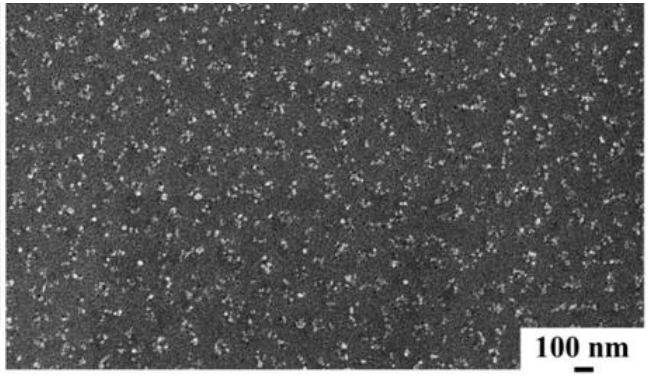

Increasing Thickness: Nucleation, Coalescence, Growth (Volmer-Weber)

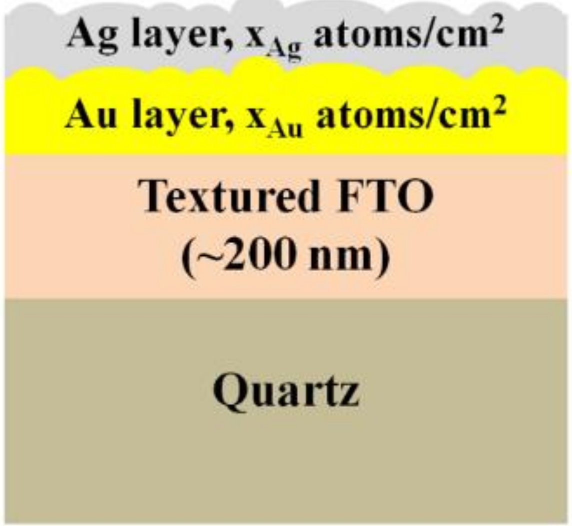
Ag layer, x_{Ag} atoms/cm^2

Au layer, x_{Au} atoms/cm^2

Textured FTO
(~200 nm)

Quartz

Au 15 nm-Ag 38 nm/FTO

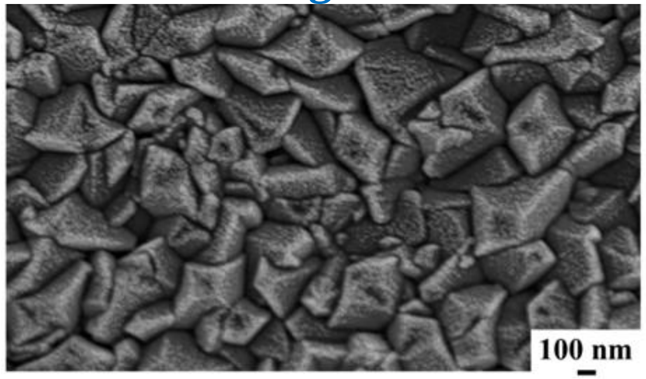

Au 7.7 nm-Ag 50 nm/FTO

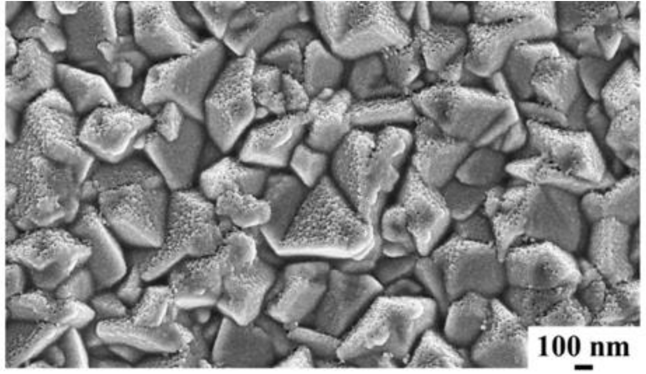

Au 31 nm-Ag 41 nm/FTO

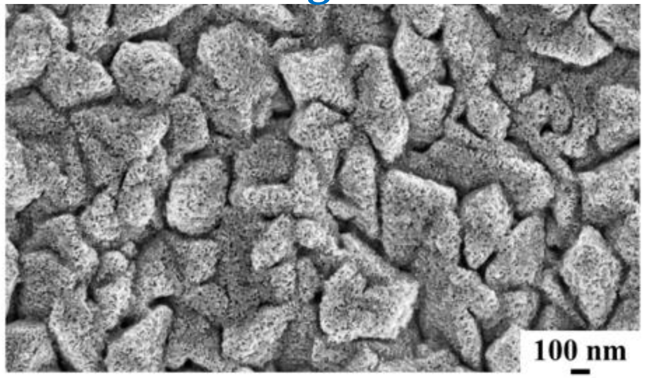

Samples Preparation and Characterization

Au-Ag Bilayers Alloying and Dewetting

Thermal-induced dewetting

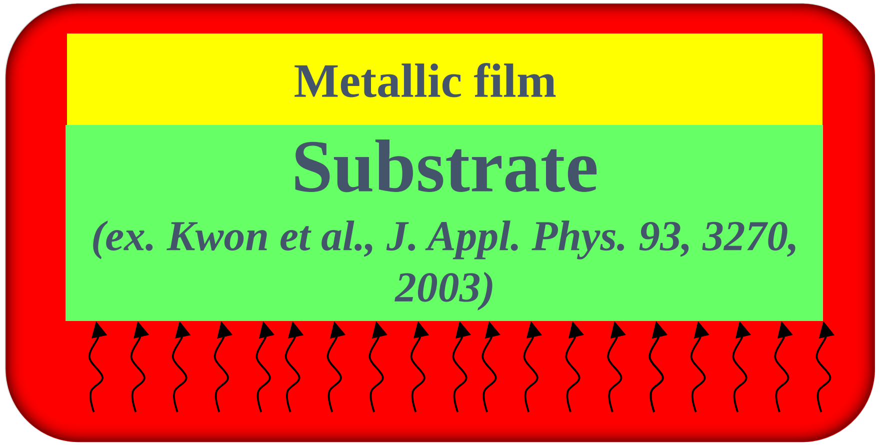

Metallic film

Substrate

(ex. Kwon et al., J. Appl. Phys. 93, 3270, 2003)

Laser beam-induced dewetting (in the liquid phase)

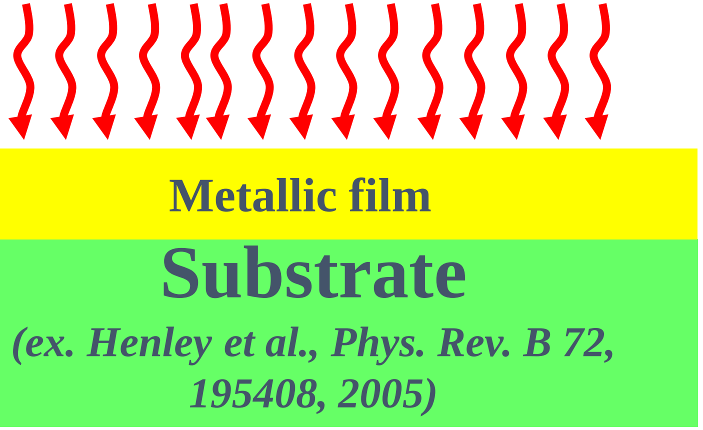

Metallic film

Substrate

(ex. Henley et al., Phys. Rev. B 72, 195408, 2005)

Metal Films on non-wetting Substrates

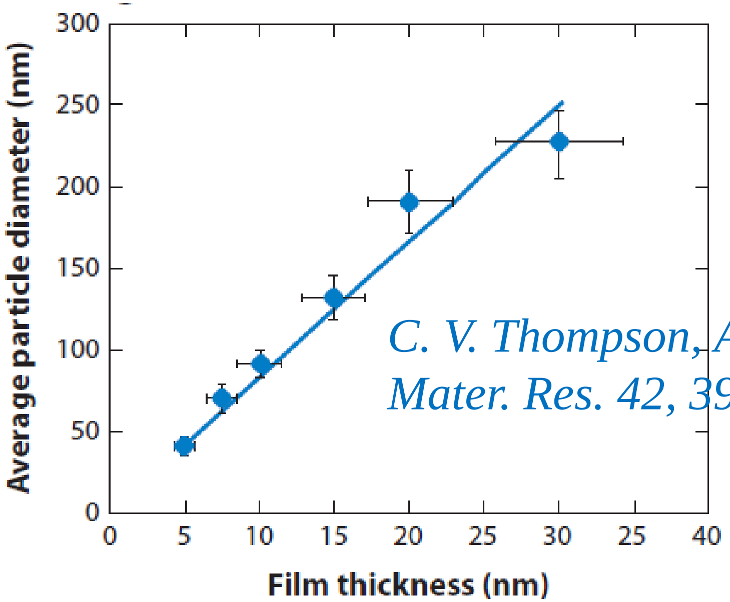

C. V. Thompson, Annu. Rev. Mater. Res. 42, 399 (2012)

Samples Preparation and Characterization

Au-Ag Bilayers Alloying and Dewetting

Laser dewetting versus thermal dewetting

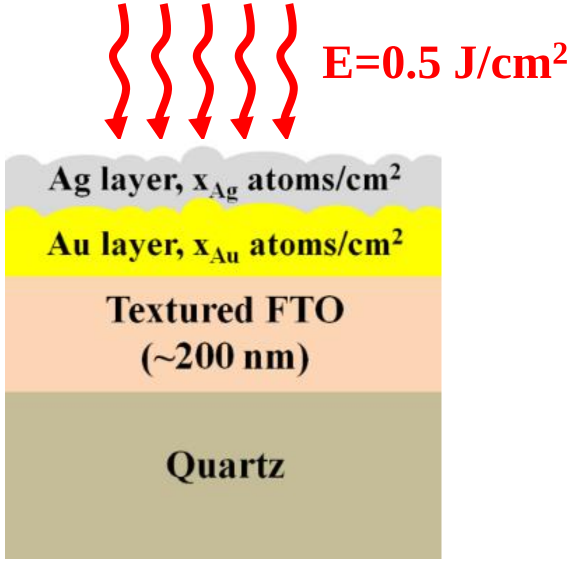
E=0.5 J/cm^2

Ag layer, x_{Ag} atoms/cm^2

Au layer, x_{Au} atoms/cm^2

Textured FTO (~200 nm)

Quartz

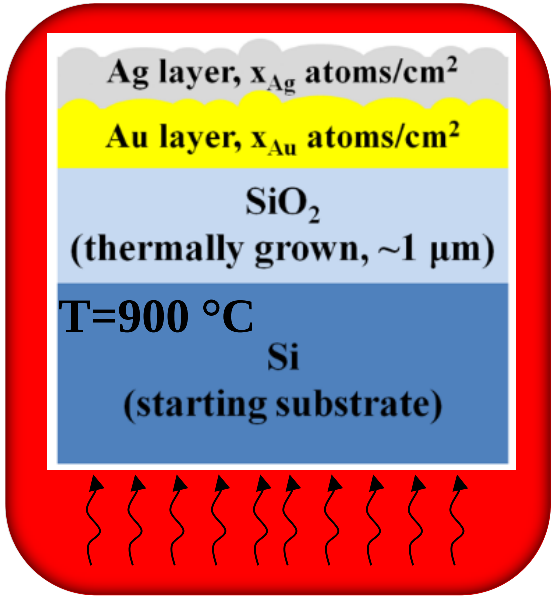
Ag layer, x_{Ag} atoms/cm^2

Au layer, x_{Au} atoms/cm^2

SiO$_2$ (thermally grown, ~1 µm)

T=900 °C

Si (starting substrate)

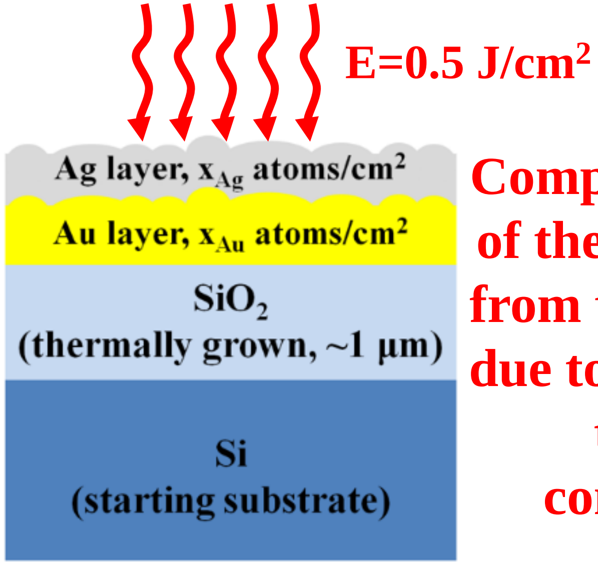
E=0.5 J/cm^2

Ag layer, x_{Ag} atoms/cm^2

Au layer, x_{Au} atoms/cm^2

SiO$_2$ (thermally grown, ~1 µm)

Si (starting substrate)

Complete Ablation of the Metal Films from the Substrate due to the SiO$_2$ low thermal conductivity

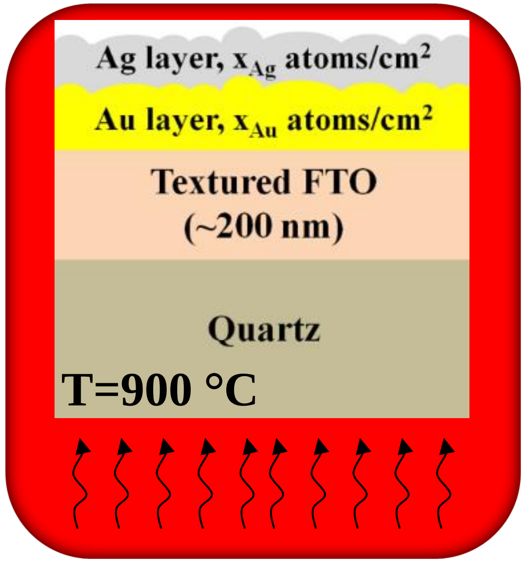
Ag layer, x_{Ag} atoms/cm^2

Au layer, x_{Au} atoms/cm^2

Textured FTO (~200 nm)

Quartz

T=900 °C

Sample	Sheet Resistance (Ω/sq)
FTO	8.6
FTO-1.0 J/cm^2	8.1
FTO_Au5nm_1.0 J/cm^2	7.5
FTO_Au10nm_1.0 J/cm^2	7.5
FTO_Au10nm_500 °C 3h	19.7

Samples Preparation and Characterization

Au-Ag Bilayers Alloying and Dewetting

Au-Ag Solid State Alloying and Dewetting

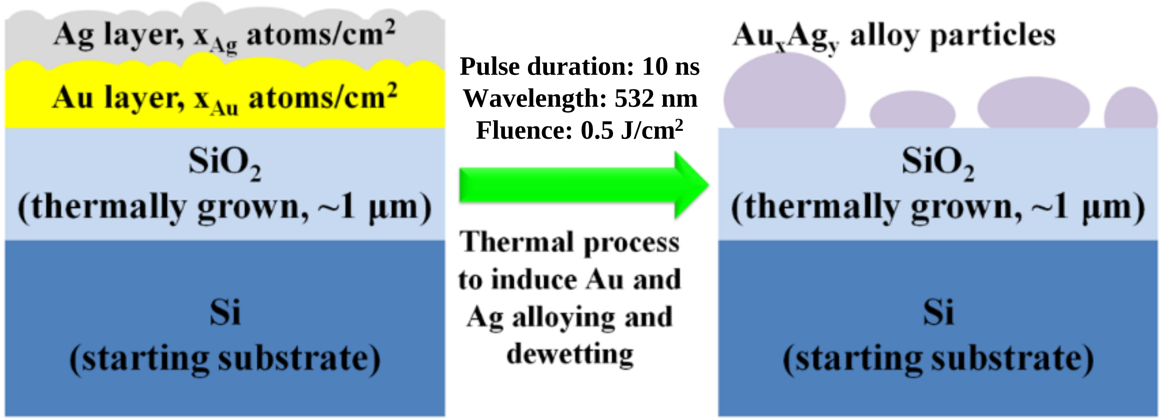

Ag layer, x_{Ag} atoms/cm^2

Au layer, x_{Au} atoms/cm^2

SiO_2
(thermally grown, ~1 µm)

Si
(starting substrate)

Pulse duration: 10 ns
Wavelength: 532 nm
Fluence: 0.5 J/cm^2

Thermal process to induce Au and Ag alloying and dewetting

Au_xAg_y alloy particles

SiO_2
(thermally grown, ~1 µm)

Si
(starting substrate)

Au-Ag Liquid State Alloying and Dewetting

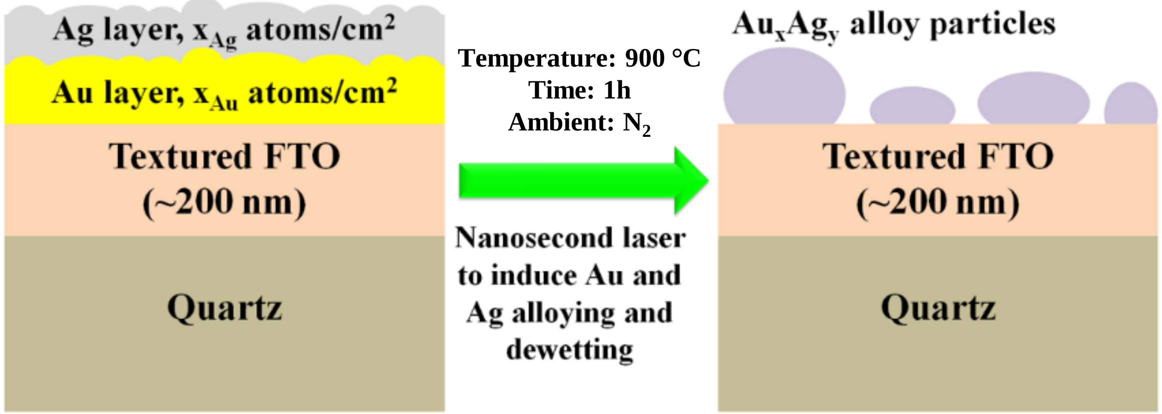

Ag layer, x_{Ag} atoms/cm^2

Au layer, x_{Au} atoms/cm^2

Textured FTO
(~200 nm)

Quartz

Temperature: 900 °C
Time: 1h
Ambient: N_2

Nanosecond laser to induce Au and Ag alloying and dewetting

Au_xAg_y alloy particles

Textured FTO
(~200 nm)

Quartz

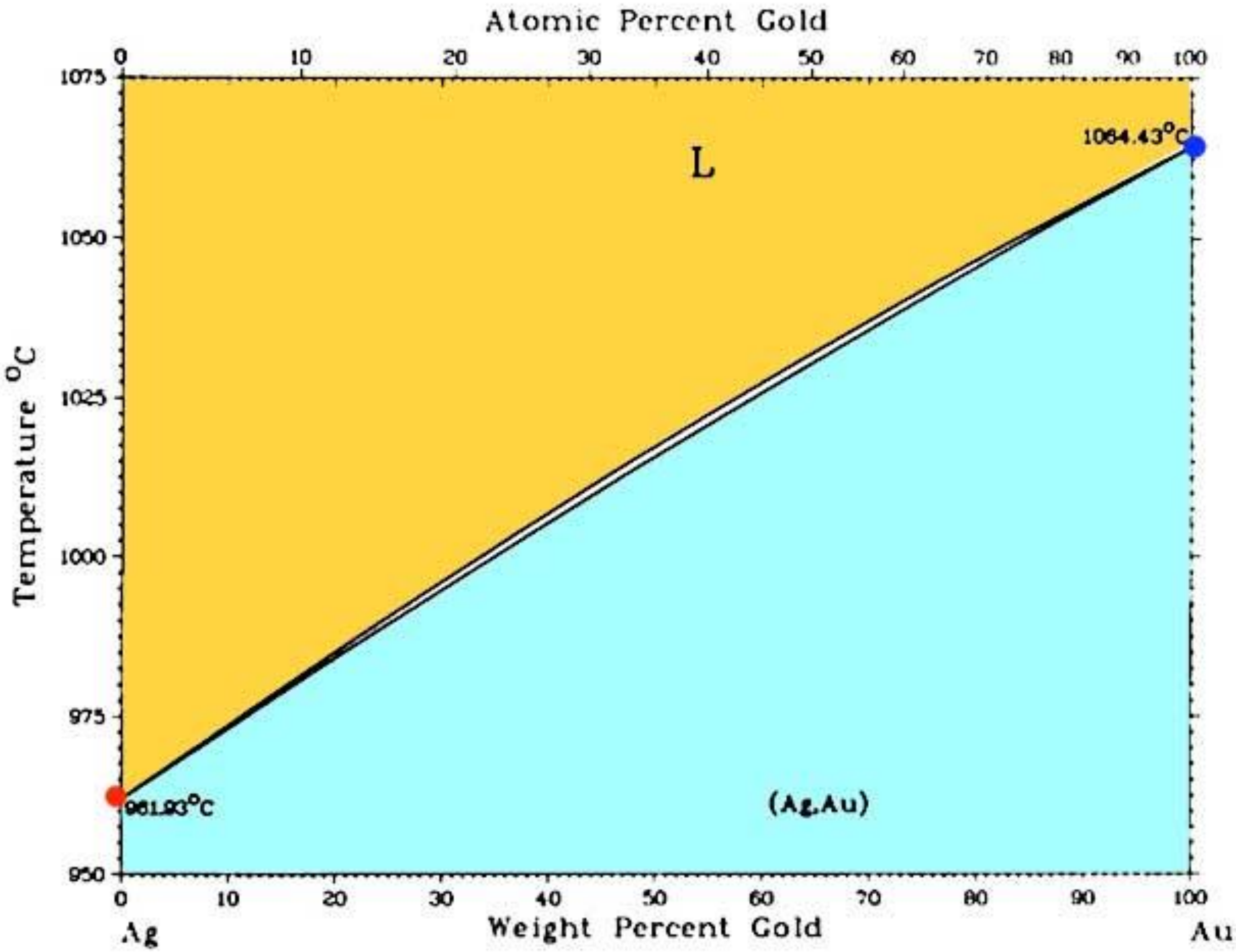

Phase diagram for Au-Ag is a simple lens type. the FCC phase shows complete solid solubility

Samples Preparation and Characterization

Au-Ag Bilayers Alloying and Dewetting

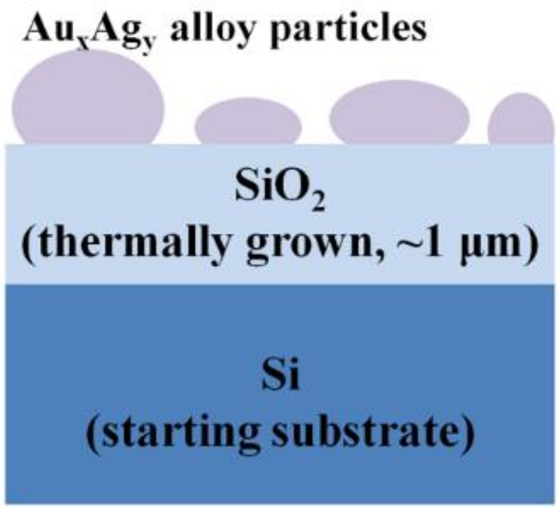

Au_xAg_y alloy particles

SiO_2
(thermally grown, ~1 µm)

Si
(starting substrate)

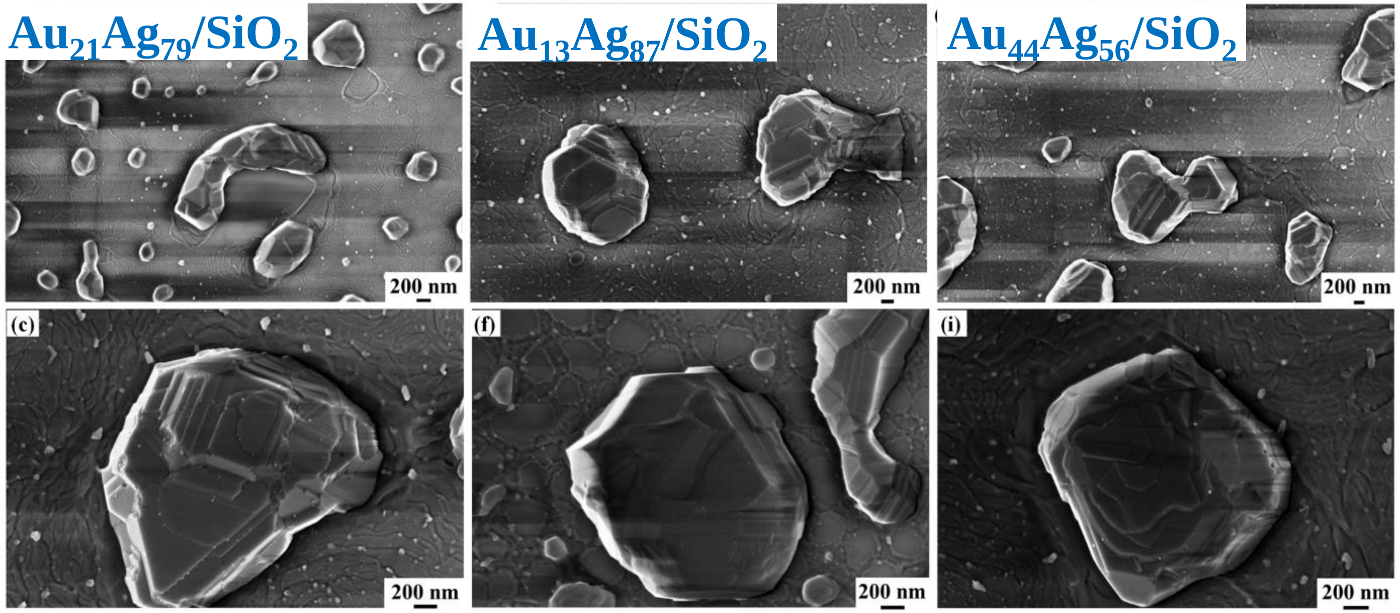

Au-Ag Solid State Alloying and Dewetting: Faceted Particles

Au-Ag Liquid State Alloying and Dewetting: Spherical Particles

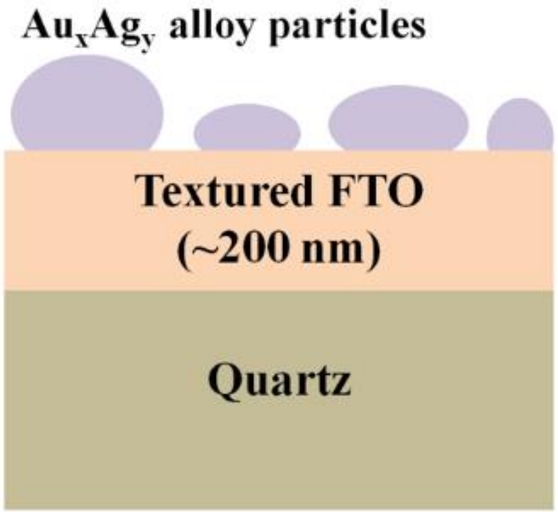

Au_xAg_y alloy particles

Textured FTO
(~200 nm)

Quartz

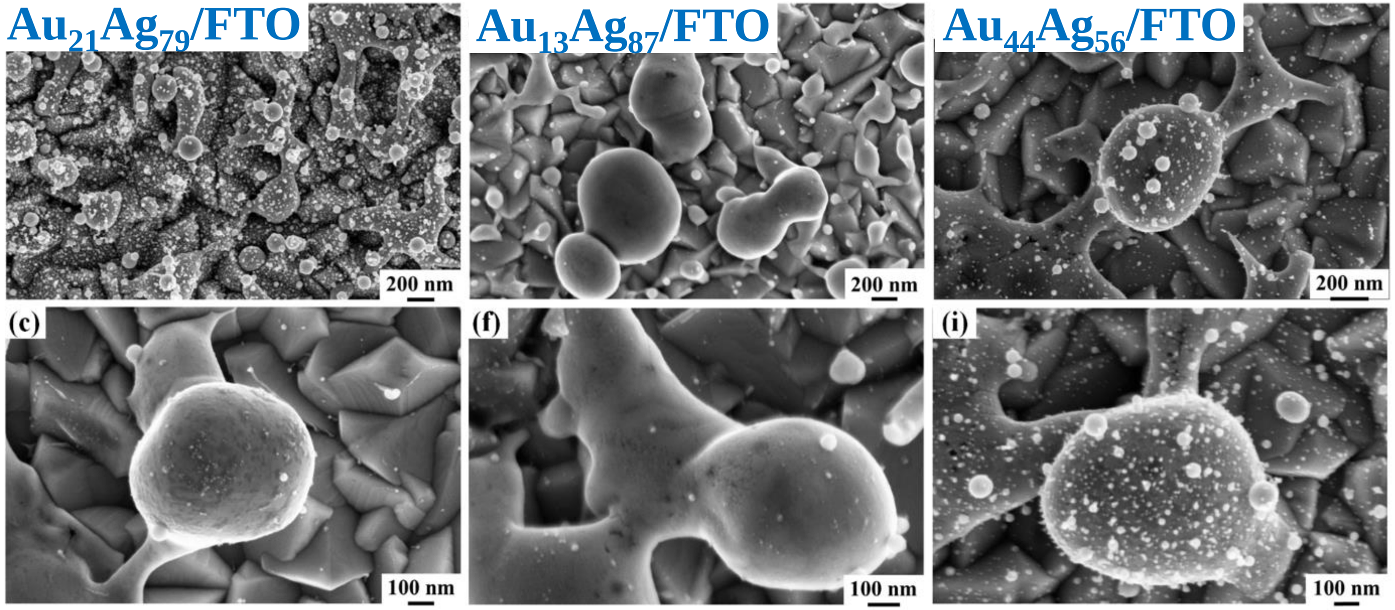

Samples Preparation and Characterization

Au-Ag Particles Dealloying

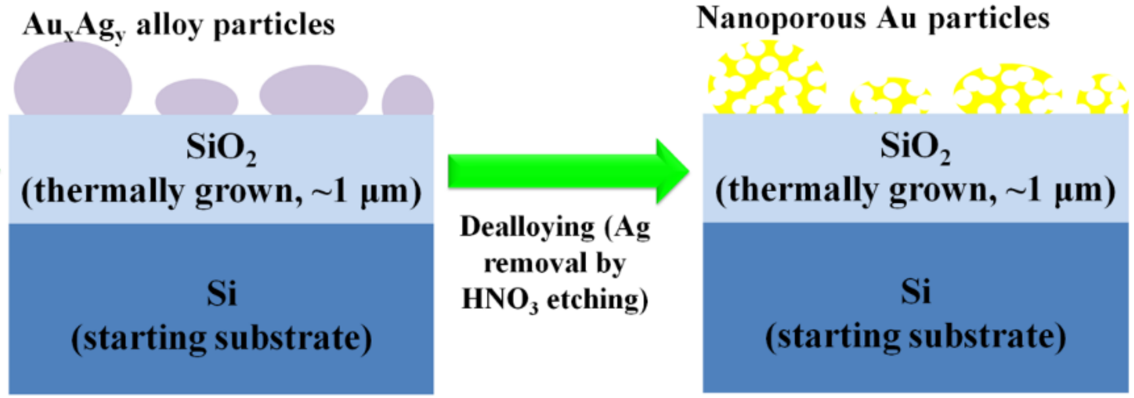

Au_xAg_y alloy particles

SiO_2
(thermally grown, ~1 µm)

Si
(starting substrate)

Dealloying (Ag removal by HNO_3 etching)

Nanoporous Au particles

SiO_2
(thermally grown, ~1 µm)

Si
(starting substrate)

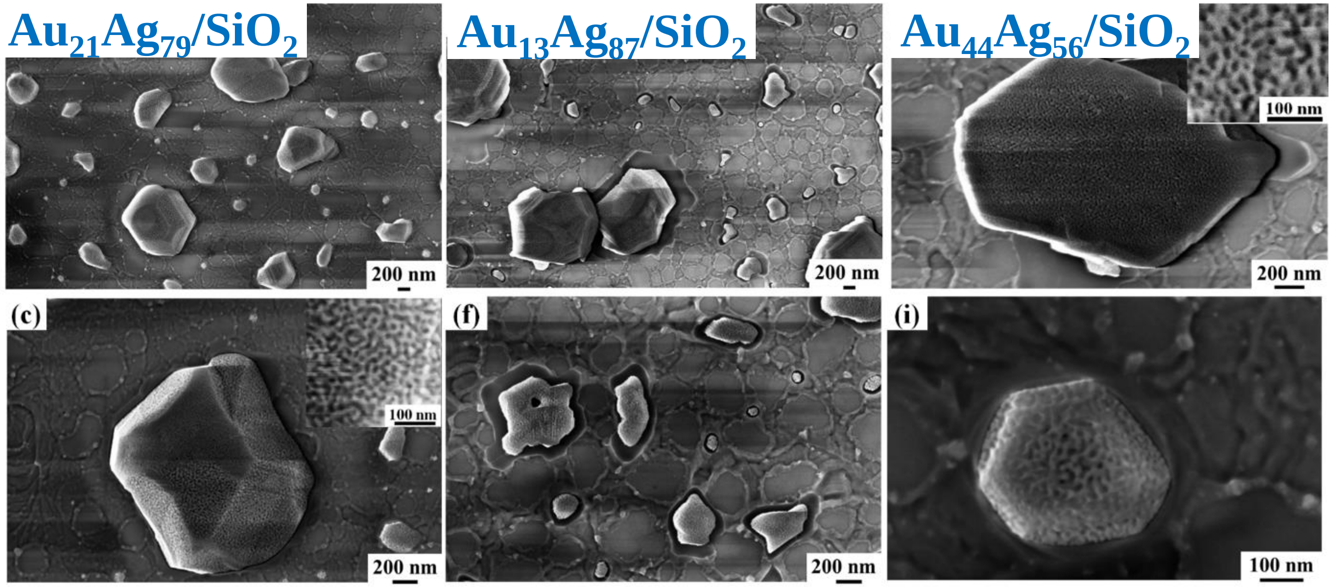

Dealloying in 70%-HNO_3 for 20 min

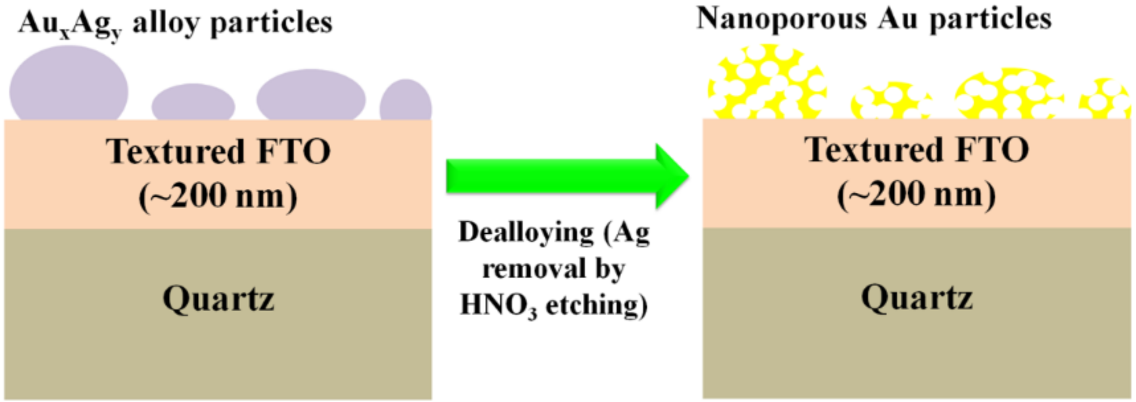

Au_xAg_y alloy particles

Textured FTO
(~200 nm)

Quartz

Dealloying (Ag removal by HNO_3 etching)

Nanoporous Au particles

Textured FTO
(~200 nm)

Quartz

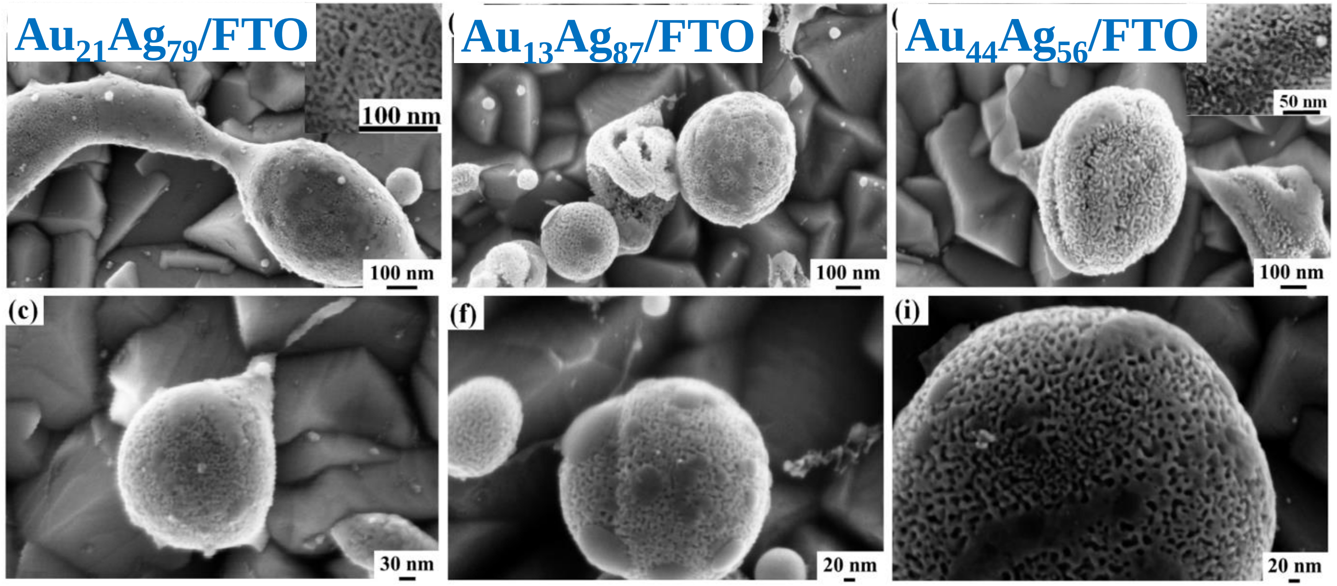

Results and Discussion

Particles Size

Before Dealloying

After Dealloying

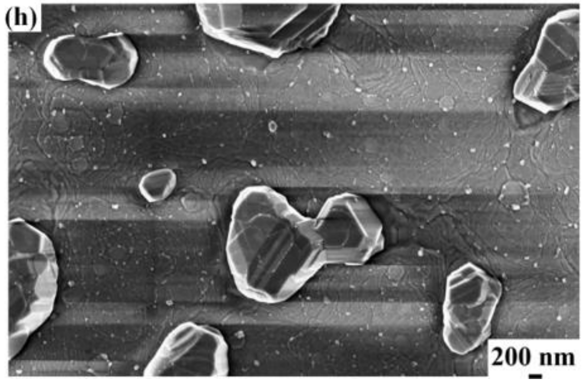

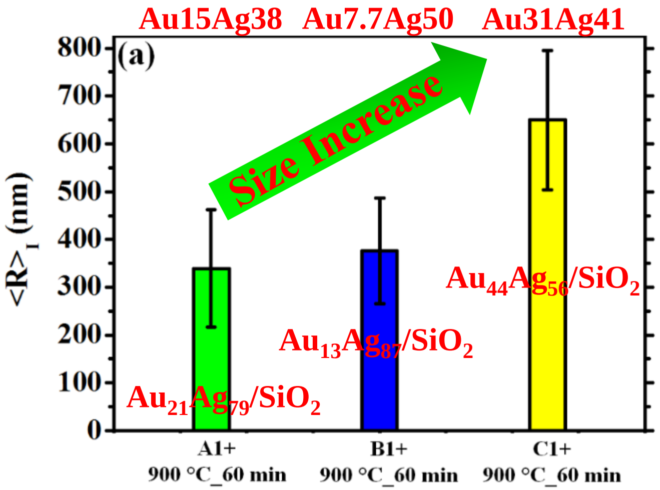

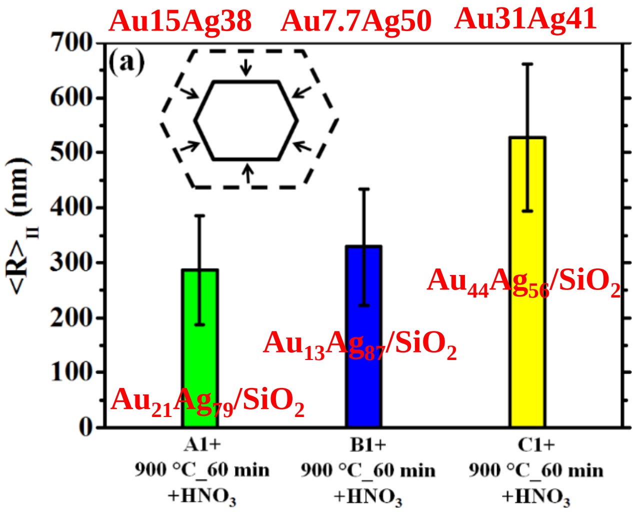

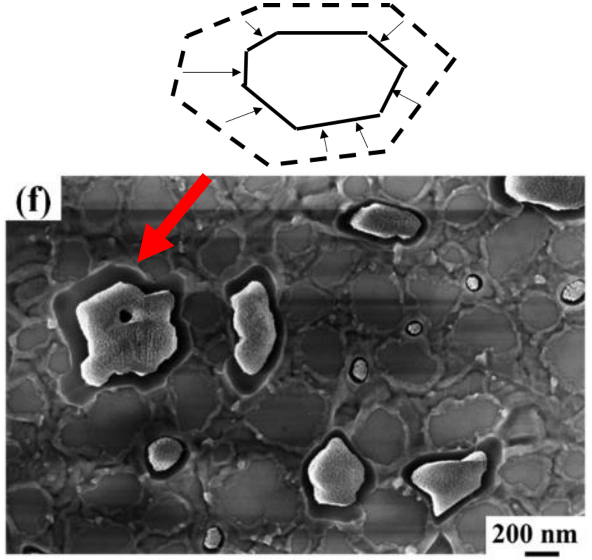

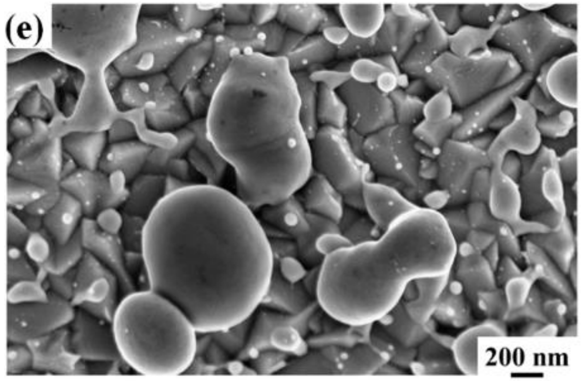

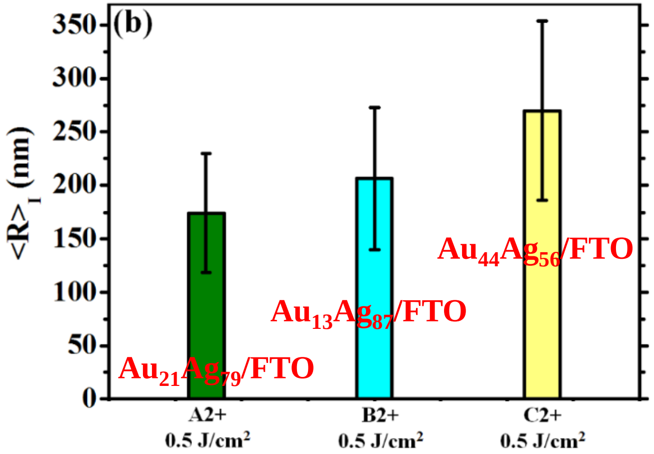

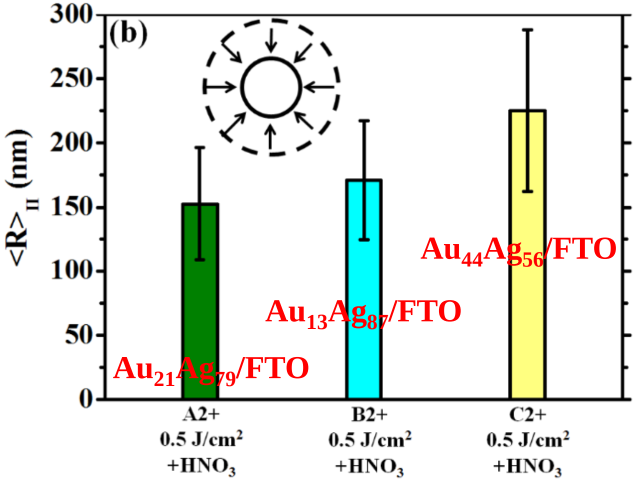

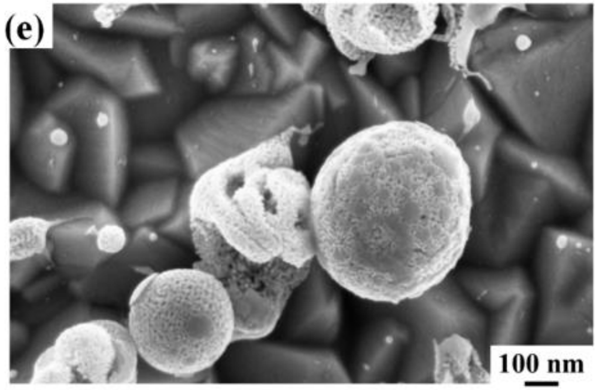

40% Volume Particles Shrinkage after Dealloying

Results and Discussion

Particles Porosity

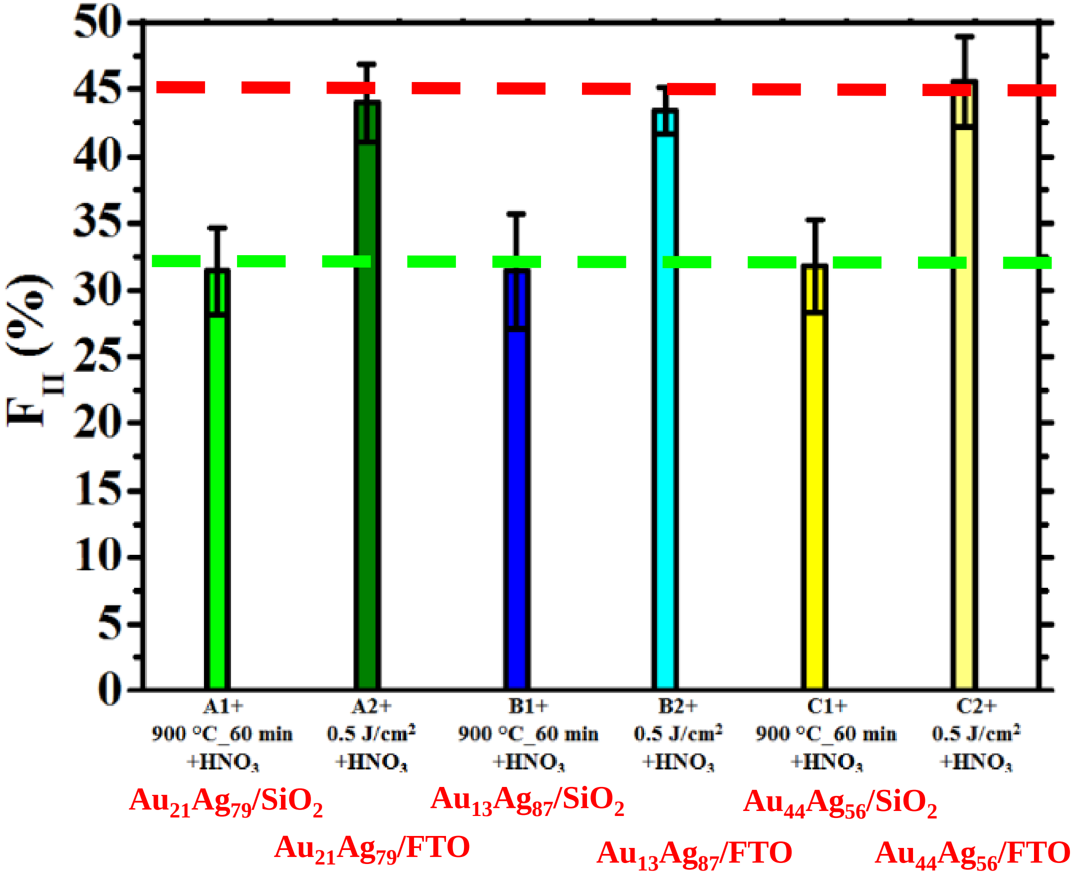

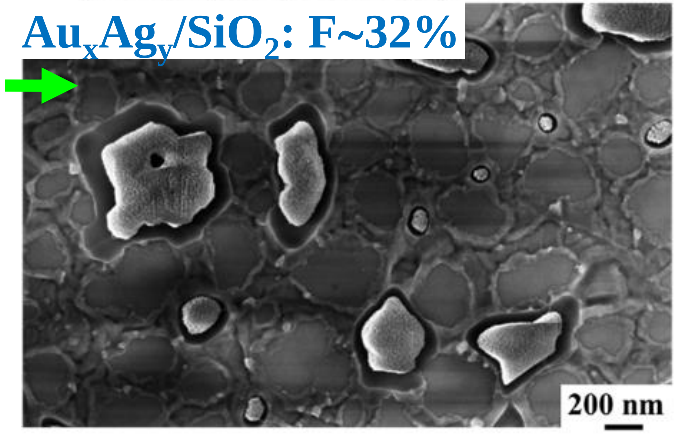

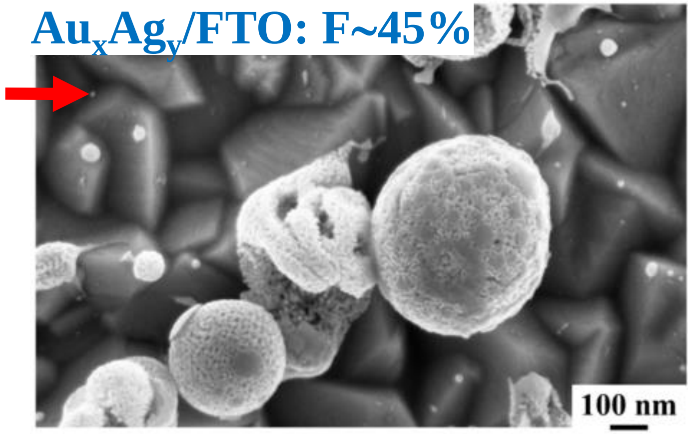

Hypothesis:
Molten-Phase Alloying: Au and Ag atoms in the particles could be more homogeneously (randomly) distributed

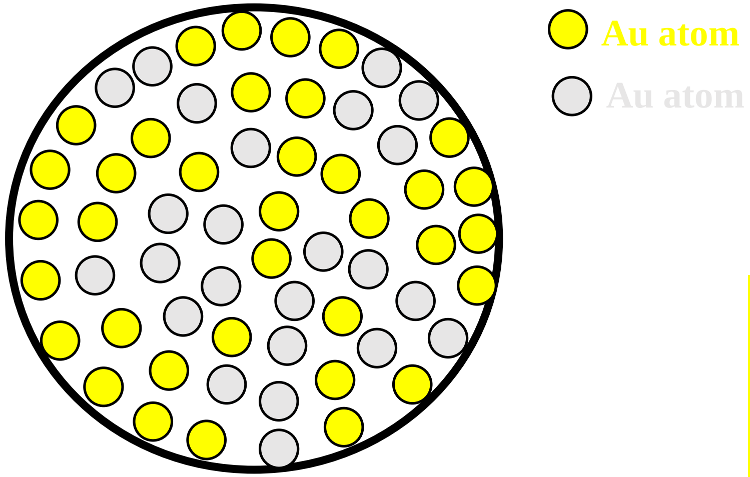

Solid-State Alloying

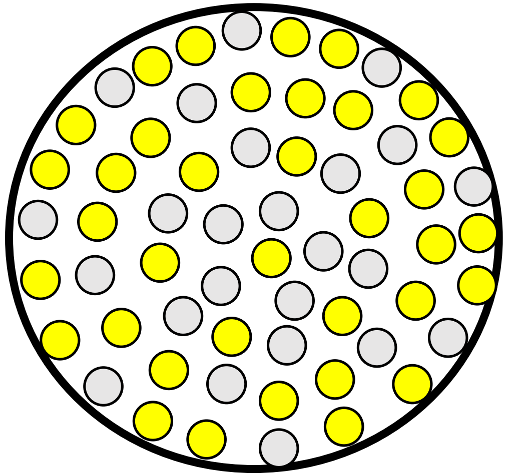

Molten-Phase Alloying: Better Homogeneity?
(Under Investigation by STEM)